EFFECTS OF NANOCLAYS AND FIBER ON RHEOLOGICAL AND MECHANICAL PROPERTIES OF 3D PRINTABLE CEMENT-BASED MORTARS

by

Ata Nikravan

B.S., Civil Engineering, Islamic Azad University of Tabriz, 2006

Submitted to the Institute for Graduate Studies in
Science and Engineering in partial fulfillment of
the requirements for the degree of
Master of Science

Graduate Program in Civil Engineering
Boğaziçi University

2023

ACKNOWLEDGEMENTS

First of all, I would like to thank my supportive professor and thesis supervisor Prof. Nilufer Özyurt Zihnioğlu who had faith in me and gave me a chance to pursue master's studies after many years. I truly appreciate her consistent guidance on many occasions throughout my studies and thesis work.

I would like to acknowledge Assoc. Prof. Zeynep Başaran Bundur for being an incredible advisor who allowed me to join her research group in a TÜBİTAK project and let me conduct many experiments at the laboratory of Özyeğin University.

I am thankful to the Scientific and Technical Research Council (TÜBİTAK) of Turkey for providing financial support for our project (MAG-119M520).

I am grateful to the assistants of the construction materials laboratory Onur Öztürk and Olcay Gürabi Aydoğan. I would never forget Mr. Ümit Melep who was always there for me and provided a comfortable atmosphere to conduct my experiments in the laboratory.

Very special thanks to our research group members Mina Aydın and Tolga Aydın for their cooperation. I am also grateful to my colleagues Nilhan Andiç, Elifsu Balcı, and Can Gürer Yücel for their support. We learned many things together.

Finally, I am extremely thankful for my lovely father, mother, and my kind brother who supported me in all aspects and built my confidence to pursue my study abroad. I would not be able to accomplish and complete my study without my family's kind support.

ABSTRACT

EFFECTS OF NANOCLAYS AND FIBER ON RHEOLOGICAL AND MECHANICAL PROPERTIES OF 3D PRINTABLE CEMENT-BASED MORTARS

Despite the many advantages of 3D printing (3DP), it is less adapted to construction. Finding the right materials and evaluating their properties are still the main barriers to implementing this novelty in construction. In this study, Sepiolite (SEP) and Nano-Montmorillonite (NM) Nano-clays are investigated as rheological modifiers in pre-designed cement-based mortar tailored for 3D concrete printing (3DCP) modified with fly ash (FA) to fulfill sustainability. Moreover, Polyamide (PA) fiber addition is evaluated as reinforcement. Experiments were carried out to assess effect of the addition of NM and SEP at rates of 0.5% and 1% (by weight of binder amount), and PA fiber at rates of 0%, 0.05%, 0.125%, and 0.150% (by weight of binder amount), on the properties of printable concrete. In total, five different mix designs were either extruded manually using a caulk gun or printed using a robot, depending on the type of the experiment. Additionally, concrete samples were cast for some of the experiments to evaluate the effect of printing on the properties of the mortar. Based on the obtained results, PA fiber with a content ratio of 0.15% improved interlayer bonding and reduced slump flow loss progress as well. Moreover, the addition of 1% NM/SEP decreased workability as expected, but improved buildability, appearance, and interlayer bonding. Replacing 20% of cement by FA enhanced rheological characteristics, but weakened buildability and accelerated the slump flow loss trend.

ÖZET

3 BOYUTLU YAZDIRILABILIR ÇİMENTO BAZLI HARÇLARDA NANO KİLLERİN VE LİFLERİN REOLOJİKK VE MEKANİK ÖZELLİKLER ÜZERİNE ETKİLERİ

3D baskının (3DP) birçok avantajına rağmen, inşaat sektörüne daha az adapte olmuştur. Doğru malzemeleri bulmak ve özelliklerini değerlendirmek, bu yeniliğin inşaatta uygulanmasının önündeki ana engeller olmaya devam etmektedir. Bu çalışmada, Sepiolit (SEP) ve Nano-Montmorillonit (NM) Nano-killer, sürdürülebilirliği sağlamak için uçucu kül (FA) ile modifiye edilmiş 3D beton baskı (3DCP) için uyarlanmış önceden tasarlanmış çimento bazlı harçta reolojik değiştiriciler olarak araştırılmıştır. Ayrıca, Poliamid (PA) fiber ilavesi takviye olarak değerlendirilmiştir. Bağlayıcı miktarının ağırlığına göre %0,5 ve %1 oranlarında NM ve SEP ile bağlayıcı miktarının ağırlığına göre %0, %0,05, %0,125 ve %0,150 oranlarında PA fiber ilavesinin basılabilir betonun özellikleri üzerindeki etkisini değerlendirmek için deneyler gerçekleştirilmiştir. Toplamda beş farklı karışım tasarımı, deneyin türüne bağlı olarak ya bir kalafat tabancası kullanılarak manuel olarak ekstrüde edilmiş ya da bir robot kullanılarak basılmıştır. Ayrıca, baskının harcın özellikleri üzerindeki etkisini değerlendirmek amacıyla bazı deneyler için beton numuneleri dökülmüştür. Elde edilen sonuçlara göre, %0,15 içerik oranına sahip PA fiber, katmanlar arası bağlanmayı iyileştirmiş ve çökme akış kaybı ilerlemesini de azaltmıştır. Ayrıca, %1 NM/SEP ilavesi beklendiği gibi işlenebilirliği azaltmış, ancak inşa edilebilirliği, görünümü ve tabakalar arası bağlanmayı iyileştirmiştir. Çimentonun %20'sinin FA ile değiştirilmesi reolojik özellikleri geliştirmiş, ancak inşa edilebilirliği zayıflatmış ve çökme akış kaybı eğilimini hızlandırmıştır.

TABLE OF CONTENTS

ACKNOWLEDGEMENTS . . . iii
ABSTRACT . . . iv
ÖZET . . . v
LIST OF FIGURES . . . viii
LIST OF TABLES . . . xii
LIST OF ACRONYMS/ABBREVIATIONS . . . xiv
1. INTRODUCTION . . . 1
1.1. 3DP Methods in Construction . . . 2
1.1.1. Binder Jetting . . . 2
1.1.2. Material Deposition Method (MDM) . . . 3
1.2. Required Properties for Printable Concrete . . . 4
1.2.1. Rheological Characteristics . . . 4
1.2.2. Mechanical Characteristics . . . 5
1.3. Required Materials for 3DCP . . . 6
1.4. Pumping and Printing Systems . . . 10
2. MATERIALS AND METHODS . . . 12
2.1. Materials . . . 12
2.1.1. Cement . . . 12
2.1.2. Fly Ash . . . 13
2.1.3. Aggregates . . . 15
2.1.4. Clay . . . 16
2.1.5. Plasticizer Admixture . . . 17
2.1.6. Fiber . . . 17
2.2. Mixture Design . . . 18
2.2.1. Preparation of the Mixes . . . 18
2.3. Experimental Methods . . . 19
2.3.1. Printing Equipment . . . 19
2.3.2. Preliminary Tests . . . 20

2.3.2.1. Fiber Distribution 20
2.3.2.2. Extrudability 21
2.3.3. Fresh State Tests 21
2.3.3.1. Flowability Test 21
2.3.3.2. Buildability/Stability Test 22
2.3.4. Hardened State Tests 24
2.3.4.1. Compressive Strength Test 24
2.3.4.2. Interlayer Bonding Strength Test 25
2.3.4.3. Flexural Strength Test 31
3. RESULTS AND DISCUSSION 33
3.1. Preliminary Test Results 33
3.1.1. Fiber Distribution 33
3.1.2. Extrudability 35
3.2. Fresh State Test Results 36
3.2.1. Flowability Test Results 36
3.2.1.1. Determining SP Amount 36
3.2.1.2. Evaluating flowability of non-reinforced mixtures . . 37
3.2.1.3. Evaluating flowability of fiber-reinforced mixtures . . 41
3.2.2. Buildability Test Results 48
3.3. Hardened State Test Results 51
3.3.1. Compressive Strength Test Results 51
3.3.2. Interlayer Bonding Test Results 56
3.3.2.1. Interlayer bond strength dog bone shaped specimens 56
3.3.2.2. Interlayer bond strength of the printed specimens . . 57
3.3.3. Flexural Strength Test Results 62
3.3.3.1. Flexural strength of the cast specimens 62
3.3.3.2. Flexural Strength of the Printed Specimens 63
4. CONCLUSION 66
4.1. Future Work 69
REFERENCES 70

LIST OF FIGURES

Figure 2.1. Cement (OPC-CEM 42.5R), FA-SEP particle size distribution. . . 15

Figure 2.2. Cumulative percent passing of the aggregate. 16

Figure 2.3. Printing setup. 19

Figure 2.4. Sample preparation for fiber distribution test. 20

Figure 2.5. The schematic view of the process flow used for extrudability. . . . 21

Figure 2.6. Control mix. 22

Figure 2.7. Buildability test setup. 23

Figure 2.8. Measuring the height of the printed specimen for stability test. . . 23

Figure 2.9. Sample preparation steps for compression test. 25

Figure 2.10. Preparing samples for direct tensile test. 26

Figure 2.11. Preparing samples for interlayer bonding test. 27

Figure 2.12. Loading additional weight on top of the samples of interlayer bonding test. 28

Figure 2.13. Utilizing pigment in one layer. 29

Figure 2.14. Preparing samples for the MTS test. 29

Figure 2.15. Direct tensile test setup. 30

Figure 2.16. Section analysis after failure by Image J software. 30

Figure 2.17. 3-Point bending specimens. 31

Figure 2.18. 3-Point bending test setup. 32

Figure 3.1. Fiber clump problem in 0.15% volume. 33

Figure 3.2. Distribution of PA fibers in dry mix. 34

Figure 3.3. Distribution of PA fiber in crushed mortar. 35

Figure 3.4. Results of flow table test for control mix with various SP amount. 36

Figure 3.5. Results of flow table test for SEP_0.5_FA with various SP amount. 37

Figure 3.6. Result of flow table test for mix designs without fiber. 38

Figure 3.7. Effect of NM content on flowability. 40

Figure 3.8. Effect of SEP content on flowability. 40

Figure 3.9. Flow table test results for CONTROL mixes containing different dosages of PA fibers. 42

Figure 3.10. Flow table test results for CONTROL_FA mixes containing different dosages of PA fibers. 43

Figure 3.11. Results of flow table tests for mix designs containing 0.125% PA fiber. 44

Figure 3.12. Flow Table tests conducted for CONTROL_FA. 45

Figure 3.13. Flow loss of clay containing samples in different dosages of PA fibers in a 2-hour period. 46

Figure 3.14. Failure of the structure during printing of the 6^{th} layer. 48

Figure 3.15. Printed samples for buildability test 2 hours after printing. 49

Figure 3.16. Total height of the samples at the beginning and end of the buildability test. 51

Figure 3.17. Compressive strength of printed samples with 5 min time intervals at 28 days. 52

Figure 3.18. Compressive strength of printed samples with 30 min time intervals at 28 days. 53

Figure 3.19. Compressive strength comparison between 5/30 min time interval. 54

Figure 3.20. Compressive strength comparison between cast/printed samples. . 55

Figure 3.21. Schematic view of prepared samples. 55

Figure 3.22. Section view of the crushed specimens under compression test and crack development pattern in y-z and x-z planes. 56

Figure 3.23. Interlayer bonding test results for dog-bone-shaped samples. . . . 57

Figure 3.24. Interlayer bonding result for the printed samples-the time gap between the 2 layers was 30 min. 58

Figure 3.25. Interlayer bonding results for the printed samples after improvement of interlayer by application of cement paste. 59

Figure 3.26. Interlayer bonding results for the printed samples before and after improvement of interlayer by application of cement paste. 60

Figure 3.27. The effect of printing time gap on interlayer bonding strength-control specimen. 61

Figure 3.28. Uniaxial tensile test result. 62

Figure 3.29. Fiber content effect on the flexural strength of cast sample. 63

Figure 3.30. Printed beams ready for the 3-point bending test. 64

Figure 3.31. Fracture failure of the printed beams after conducting three-point bending test. 64

Figure 3.32. Flexural strength of the printed samples. 65

LIST OF TABLES

Table 2.1. Physical properties of cement 12

Table 2.2. Mechanical properties of cement 12

Table 2.3. Chemical properties of cement 13

Table 2.4. Physical properties of FA 14

Table 2.5. Chemical properties of FA 14

Table 2.6. Properties of PA microfibers 17

Table 2.7. Mix Designs (%) 18

Table 3.1. Extrudability results for different fiber lengths. 35

Table 3.2. Flow table test results for mix designs without fiber. 38

Table 3.3. Flow table test results for NM and SEP containing Mixtures . . . 39

Table 3.4. Flow table test results for CONTROL mixes containing different dosages of PA fibers 42

Table 3.5. Flow table test results for CONTROL_FA mix containing different dosage PA fibers 43

Table 3.6. Flow Table test results for mix designs with 0.125% PA fiber . . . 45

Table 3.7. Flow loss of clay containing samples in different dosages of PA fibers in a 2-hour period 47

Table 3.8. The layer height of the samples immediately after printing 49

Table 3.9. Total final height obtained for mix designs after buildability test . 50

Table 3.10. Percent change of height occurred for different samples at the buildability test. 51

Table 3.11. Flexural strength test results of samples at 28-day age. 65

LIST OF ACRONYMS/ABBREVIATIONS

3DCP	3D Concrete Printing
3DP	3D Printing
BJ	Binder Jetting
CAD	Computer-Aided Design
CC	Contour Crafting
DCP	Digital Construction Platform
FA	Fly Ash
GDP	Gross Domestic Product
LS	Lignosulfonate
MDM	Material Deposition Method
NM	Montmorillonite
OPC	Ordinary Portland Cement
PA	Polyamide
PCE	Polycarboxylate Ether
PNS	Polynaphthalene Sulfonate
SEP	Sepiolite
SP	Superplasticizers
VMA	Viscosity Modifying Agent
W/B	Water to Binder

1. INTRODUCTION

The construction sector as one of the largest industries in the world with 6% of the global Gross domestic product (GDP), has a significant impact on the world economy. Despite this large share and influence, this sector is still suffering from a lack of modern technologies and novelty compared to other large industries. Generally, construction gets lower investment for novelty and new technologies. For instance, in the U.S. only 1.5% of the value added of construction is invested in technology, while this number is 3.3% for the manufacturing industry and 3.6% for the economic sector. There have been several advances and progress in the construction industry in recent decades, but still companies and researchers are trying to increase their efficiency and improve their building methods. Industry 4.0 has introduced digitalization to the construction sector to improve sustainability and efficiency. Based on the literature review, the construction field is slowly adapting automated systems and robotic science, and most modern technologies like 3DP have been used for a very specific purpose. Especially due to the exclusive nature of projects in the construction industry, duplication of these novel technologies in multiple projects are not possible yet, unlike other industries [1, 2].

3DP as an additive manufacturing and rapid prototyping technique is one of the innovative technologies of industry 4.0 which is utilized to generate complex 3D geometries from a designed model by computer. It enables project managers to bring flexibility by producing complex geometries and various objects and changing the methods of doing projects. This automated process utilizes a computer-aided design (3D-CAD) to generate a structure, with limited human contribution, so unlike traditional construction, which is labor intensive, 3DP requires low manual work which results in a reduction in waste of material and labor needs. The 3DP process is a design-free technique for joining materials layer upon layer through extrusion using a print head or nozzle to create an object from a 3D model [2-4].

There are many other benefits to using 3DP as a modern building technique. First, 3DP eliminates the need for formwork which included about 10% of the cost of concrete work, so it can save time and money without the need for installing formwork. Second, as a safe method, it can be used in dangerous projects, where the labor force's health might be in danger. In addition to a lower rate of injuries, labor costs will be minimized. Then, projects can be completed in a shorter time, since the printing action by a robot is much faster than traditional building techniques by using human force. Moreover, it increases sustainability as an environmentally friendly technique due to its precise work and generating less waste compared to human work. Finally, thanks to its architectural freedom, it enables engineers to get benefitted from sophisticated designs. It was introduced to construction by Pegna from Rensselaer Polytechnic Institute in 1997. Then, Loughborough University defined "Concrete Printing" concept for the first time at 2003 [5].

1.1. 3DP Methods in Construction

3DP in the construction industry can be classified into two styles based on the utilized methods, called binder jetting (BJ) and material deposition method (MDM). Both methods are executed based on a layer-over-layer printing concept and get benefited from a 3D model designed by a computer that divides the model into several 2D layers before printing with assigned material as ink. MDM method is more popular than BJ in construction since it has more correspondence in this industry [6].

1.1.1. Binder Jetting

In this process, the printer extrudes the binder layer by layer to print a 3D element on a powder bed. The binder is dropped on a thin layer of powder material based on 2D coordinates to create one layer of the object. This process continues by bonding sections on top of each other according to the designed program. Unbounded powder material on each layer remains till the end of the printing process to support the structure of the printed object but is removed at the end of the process to be recycled

and used for the subsequent object. The printing thickness is critical in this method, since increasing the printing thickness of the layers, may hinder full penetration of the binder to underneath layers and result in weak interlayer bonding. This method is suitable to print complicated elaborate objects especially those with hollow structures [6].

1.1.2. Material Deposition Method (MDM)

As a 3DP process and similar to the BJ method, the printing is proceeded by layer-by-layer extrusion according to the designed model by the software, but there is no powder material around printed sections to support the structure. Therefore, the freshly printed material should have enough buildability characteristics to resist deformation under its own weight and the pressure of subsequent layers. This is the most regular method for 3DP in construction industry which is followed by three different automated systems including contour crafting (CC), concrete printing, Flow-based fabrication and etc [6].

Although there is high interest in the 3DP research field, there are still many barriers to bringing and utilizing it in a wide range of construction projects such as lack of support from the governmental sector and lack of building codes. But, one of the main challenges is to find and optimize the right materials for 3DP in the construction sector. Normally, plastic, metal, wax, and ceramic are used for printing in different industries. A wide range of organic and non-organic materials was investigated as printing ink for construction, but cement-based ones and Portland cement concrete are the most commonly used materials that have been studied [5].

1.2. Required Properties for Printable Concrete

1.2.1. Rheological Characteristics

The pumpability and buildability properties of the material is a critical key for 3DCP. Cementitious materials and concrete should have specific characteristics to be used for 3DP. The properties of the material such as viscosity, workability, and green strength are determining features in the fresh state [2]. The most important one is a balanced relationship between pumpability and buildability. Pumpability is required for easy extrusion from the nozzle without any clog or discontinuity. It means the cementitious mortar needs to have relatively low plastic viscosity and yield stress to obtain enough flowability to be pumped from the mixer to the hose and extruded via the nozzle head smoothly. On the other hand, to control the deformation, it should show higher plastic viscosity to be stiff enough for generating enough buildability characteristics to endure its own weight and the further layers' pressure with minimum change in its shape [2, 5].

To minimize the deformation zero-slump yet pumpable concrete is needed. To fulfill these requirements, the mix design needs to possess thixotropic characteristics to facilitate smooth extrusion and provide shape stability for the printed filaments. It means the material should have low viscosity during pumping, but show high yield stress immediately after extrusion [7]. During pumping the yield stress is generated by the pump to exceed the yield stress of the material to initiate the flow and extrude material through the nozzle. But after extrusion material needs to show a high recovery rate of viscosity and gain high yield stress larger than its weight to resist deformation and enable further layers' deposition over time. The yield stress is developed over time due to reversible physical changes in the structure as a result of the thixotropic behavior of the mortar and irreversible structural change as a result of the hydration process. Therefore, an optimum level of yield stress is required, since higher yield stress makes pumping and extrusion difficult, and a lower level of yield stress and plastic viscosity weakens buildability characteristics [8, 9].

1.2.2. Mechanical Characteristics

As well as rheological properties, printed concrete is supposed to show acceptable mechanical properties in a hardened state. One of the critical issues is the anisotropic behavior of printed concrete which significantly impacts flexural properties. Anisotropy of the printed concrete mostly is attributed to the heterogenetic nature of printed structures which is caused by the interface between filaments. The interlayers are the weaknesses of the printed structure with considerable microporosity. The flexural strength property significantly depends on the section which is faced with the peak bending stress. If the maximum bending stress is induced at the interlayer, the flexural strength will decrease considerably, but if the peak stress is applied at the matrix of the filaments, the flexural strength can be increased even to a higher level than the flexural strength of the cast conventional concrete. That is why the interlayer bonding strength tests are one of the important experiments in the hardened state of printed concrete [4].

Based on the literature, bonding strength properties are influenced by different factors such as the thixotropic level of the mortar, accelerators, printing speed, nozzle distance, printing time gap, moisture content of the filaments, temperature, and other ambient conditions [4]. Different techniques are employed to improve structural integrity by enhancing cement-based filaments' bonding in the interlayer zone. Hosseini and Zakertabrizi [10] utilized a new polymer containing black carbon and sulfur as paste in the interlayer, Marchment [11] used cement paste as interlayer adhesive, and Guowei Ma and Muhammad Salman [12] used special mortar based on calcium sulphoaluminate cement, combined by cellulose fiber and limestone filler between the layers. Some other researchers used curing agents inside the fresh concrete to prevent moisture loss from the interlayer zone [13]. Some other researchers like Zareiyan [14] changed the geometry of the layers to improve the interlayer bonding by interlocking the layers.

1.3. Required Materials for 3DCP

Contrary to the invention of various printing methods, there are still serious obstacles and challenges to the full implementation of 3DP in concrete structures. Suitable design mix for 3D concrete, durability of materials, and fiber reinforcements are just some of the challenges in the materials field which are still hot research subjects at the academic and industrial levels [15].

Necessary characteristics for additive manufacturing such as printability, extrudability, and buildability determine the required characteristics for materials. For instance, extrudability restricts fiber application and defines aggregate size and shape. Binder composition is another example that influences on characteristics of printable concrete. Particles with more spherical shape and supplementary pozzolans such as FA improves workability and attributes in extrudability [15].

The required materials for 3DCP are almost the same as conventional materials with some changes in the size of the aggregates, proportion of binders, and introduction of new materials to improve the properties of concrete in both fresh and hardened states. Moreover, high-performance materials and additives are required, since the preparation of concrete, pumping, and extrusion of the cementitious ink are critical and each step needs its own requirement. Wide range of cement based materials are used such as geopolymer mortar, conventional mortar mix and nanoparticles mixed mortar with high content of binder [2].

Generally, Ordinary Portland cement (OPC) is used for 3DCP, due to its inherent thixotropic characteristics and flocculation behavior during hydration. Recently, researchers have focused on using supplementary cement-based materials such as FA, ground blast furnace slag, and silica fume to fulfill sustainability requirements by reducing carbon emissions from both the production and hydration process [7].

Supplementary additives contain mineral ingredients that create a secondary reaction which is known as a pozzolanic reaction. FA is one of the practical pozzolanic materials which is used in 3D-printed concrete. It impacts the rheological behavior of concrete with a significant decrease in plastic viscosity by reducing the resistance of concrete to flow. Substituting a part of cement with FA particles minimizes friction between cement particles, thanks to their spherical shape, which is known as the "ball bearing effect", so the workability of concrete is improved. On the other hand, the addition of FA, results in increased yield stress. This is caused by its fine particle size which fills the gap between cement grains and increases surface area. As a result of increased surface area, particles contact in the matrix is increased and more friction force is generated which leads to the generation of high yield stress and viscosity [16, 17].

The concrete which is used for printing is high-performance concrete which is normally fiber-reinforced and contains fine aggregates limited to the maximum size of 1-2 mm for easy extrudability, although coarse aggregate has been used in a few projects. Sand is the regular aggregate that is used for 3DCP. Moreover, the aggregate size is in direct relation with the nozzle size of the extruder to prevent clogging during printing [2, 18, 19]. The addition of fibers to 3DCP has a side-effect on workability by resulting in higher viscosity and yield stress, but based on the literature review some mechanical properties and rheological behavior of the cementitious mortar can be improved depending on the type of fiber. For instance, the flexural strength can be improved by using steel fibers. Due to the increase of yield stress as the result of fiber addition, the buildability can be improved. The effect of various fibers on concrete properties needs to be studied carefully from different points of view to ensure it does not have a significant impact on concrete properties, especially on interlayer bonding. Because it has been seen that some fibers like steel ones reduce interlayer bonding properties [19]. Moreover, most of the fibers contribute to gaining flexural strength, since it has been seen in many studies that short fibers align in the direction of flow in extrusion-based printing [20].

Much research has been done to develop fiber-reinforced concrete for 3DCP with different types of fibers to substitute conventional steel reinforcement. Polypropylene fiber has shown great performance to minimize the plastic shrinkage effect [21]. Glass fibers showed potential for improvement of mechanical strength of printed geopolymer concrete [22] and straight steel fibers enhanced the ductility [23]. Although different kinds of fibers showed considerable performance in imitating the behavior of conventional steel reinforcement, still it is not possible to eliminate entire steel bars in structural 3D printed elements. For this purpose, more research needs to be done to increase the flexural and tensile properties of 3D-printed fiber-reinforced concrete to higher levels [24].

PA fibers are chosen for this study to investigate their performance in 3DCP. PA as synthetic fiber is utilized in a wide range of industries due to its cheap price, being light, and possessing anti-corrosion characteristics. Due to these beneficial characteristics, its application in the construction industry is increasing rapidly. PA fibers improve concrete properties from different aspects. The ductility and toughness of concrete are increased by using PA fibers, but its effect on compressive strength development is not notable. The flexural and splitting tensile strength of concrete is also improved by the addition of PA fibers [25]. Despite several studies about the advantages of adding PA fibers in concrete, no remarkable and comprehensive research was found about PA fiber application in 3DCP.

To obtain lower yield stress and viscosity and to increase flowability, a wide range of superplasticizers (SP) such as lignosulfonate (LS), polynaphthalene sulfonate (PNS), and polycarboxylate ether (PCE) are used in 3DCP as a beneficial agent for rheology improvement. Since lower w/c ratios are employed for printing filaments with low porosity and high density to obtain durable concrete, it is essential to utilize SP to improve workability [26]. The efficiency of the SP and its impact on rheology largely depends on its type. For instance, Polycarboxylate based SP is more effective for minimizing plastic viscosity but less practical for decreasing yield stress in comparison with naphthalene sulphonate-based SP [16].

Clays are recognized as rheological modifiers which increase the shear rate of the mixture. They enable the structure to form a shape at rest but to break down when shear is applied, so widely used in different industries like paint production. Some types of clays such as bentonite (montmorillonite-based), kaolinite, and SEP are introduced to the construction industry as rheological modifiers and their application in concrete has been studied in different literature [26]. In one study, the beneficial impact of clays on reducing formwork pressure is discussed, due to their thixotropic behavior in the fresh state of concrete [27]. In another study, 0.5-1% is introduced as the optimum dosage of nano clay for increasing the rate of structural rebuilding and thixotropic behavior of the concrete, while higher dosages larger than 1.5% decrease the rate. Moreover, the particle size effect on water absorption and as result, its impact on the thixotropy of cement paste is investigated [28]. The negative effect of clay on the hydration of cement paste due to its water absorption potential is concluded [29]. All of these studies emphasize clay application in 3DCP to ease extrusion and help buildability characteristics as well, but rarely they focused on specific types of clays to evaluate their influence on some areas such as interlayer bonding which is studied carefully in the scope of this research.

In the previous phase of this study, a comparative study was conducted to evaluate the SP and NM impact on the rheology of unreinforced 3DCP. The results revealed that both of them contribute to enhancing dynamic yield stress and time-dependent evaluation of static yield stress, improving thixotropy and green strength of cement paste. This study showed clay addition improves buildability as well as other rheological characteristics [30], but no experiment was conducted by printing samples to evaluate the printed filaments characteristics in the fresh and specially hardened state, and no study was conducted in the scope of this project about fiber application in designed cementitious mortar by clays.

1.4. Pumping and Printing Systems

Different types of printing systems and extrusion methods are utilized for concrete printing. Rahul and Santhanam [31] devised a long slow moving piston and a cylinder with an open cap at both the bottom and top, connected to a pressure line of Argon gas to generate the required power for the extrusion of the mortar. Paper of 2.6 μm pore size as filtration was placed on two sides to hinder the separation of the liquid phase from the matrix and prevent leaving behind a dewatered and unextrudable mass. In another study conducted by Guowei Ma [32], awl-shaped screw was utilized to transfer materials to the nozzle for extrusion.

Based on the literature review, various printers are used on a lab scale to conduct the printing in 3D coordinates. The gantry structure as a widely adopted system is used to position the nozzle in XYZ Cartesian coordinates. As examples of gantry systems, Counter Crafting, Concrete Printing and D-shape can be listed. Robotic arm is the next printing system which is more modern than gantry, since they enable printing system to provide additional roll, pitch and yaw controls to the printing head. Moreover, by means of a robotic arm, tangential continuity method is applicable to generate layers of varying thickness, enable smoother transition between layers and improve the appearance of the printed element. Digital Construction Platform (DCP) is another printing system which moves robotic arm on a track driven mobile platform. Some of DCP system carry solar panels to provide power for its electrical engine [33]. In many studies simple cylindrical caulk gun or adhesives' sealant gun connected to plastic nozzles with different shapes were utilized for manual extrusion of singular filament or maximum 2 layered beam to conduct basic studies on behavior of 3DCP [34-36].

Extrudability largely depends on nozzle type and defines the required geometry for the nozzle. Moreover, nozzle shape determines the structural appearance and shape of the printed filaments. The most popular nozzle shapes are square, rectangular, circular, and elliptical. Circular nozzle performs better at corners, but lower contact area between extruded beads influences stability characteristics negatively. Moreover,

a circular nozzle improves the penetration rate slightly, due to constructing fewer flat layers. A square shape nozzle hole results in obtaining a smooth surface in printed filaments. The applied load is distributed equally in a square nozzle due to the large radius of the distribution area [8, 37].

The results indicate that incorporating 0.15% PA fiber had a positive effect on extrudability, interlayer bonding, and reduced slump flow loss, without significant side effects. Additionally, the addition of 1% NM/SEP decreased workability as expected, but improved buildability, appearance, and interlayer bonding. On the other hand, replacing 20% of cement with FA enhanced rheological characteristics, but had a negative impact on buildability and accelerated the slump flow loss trend.

2. MATERIALS AND METHODS

2.1. Materials

2.1.1. Cement

CEM I 42.5R type Portland Cement from Akçansa was used for preparing cementitious mortars as the main part of the binder. Physical, mechanical, and chemical properties of the consumed cement were given according to EN 197-1 [38] standard in Table 2.1, Table 2.2 and Table 2.3, respectively.

Table 2.1. Physical properties of cement.

Physical Properties	**Results**
Density (g/cm3)	3.13
Initial Setting Time (min)	131
Final Setting Time (min)	184
Soundness (Le Chatelier) (mm)	1
Fineness - Blaine Specific Surface (cm2/g)	3900
Fineness - Residue on 45μm sieve (%)	3.4
Fineness - Residue on 90μm sieve (%)	0.2

Table 2.2. Mechanical properties of cement.

Mechanical Properties	**Days**	**Standard (MPa)**	**Test Result (MPa)**
Early Strength	2	$\geqslant$ 20.0	30.7
	7	-	47.9
Standard Strength	28	42.5 $\leqslant$ strength $\leqslant$ 62.5	58.3

Table 2.3. Chemical properties of cement.

Chemical Characteristics		**Result**
SiO_2 Soluble (%)		18.05
Insoluble Residue (%)		0.35
Al_2O_3 (%)		4.85
Fe_2O_3 (%)		3.4
CaO (%)		62.6
MgO (%)		1.35
SO_3 (%)		3.35
Loss on Ignition (%)		3.7
Cl- (%)		0.0106
Na_2O / K_2O (%)		0.24/0.84
S.CaO - Free lime (%)		0.8
Mineralogical Composition	C_3S	67.77
	C_2S	0.73
	C_3A	7.08
	C_4AF	10.35
LSF		1.03

2.1.2. Fly Ash

Class F type FA was used in this study as a binder obtained from Çatalhöyük thermal power plant. FA is beneficial for the workability of the 3DCP by minimizing yield stress and viscosity at the early stage [39] and is vital for designing sustainable 3D printable mixes [40]. Table 2.4 and Table 2.5 summarize physical and chemical properties of FA, respectively. Cement (OPC CEM 42.5R) and FA particle size distribution were given in Figure 2.1.

Table 2.4. Physical properties of FA.

Physical properties		**Result**
Density (g/cm3)		2.1
Residue on 45μm sieve (%)		28.8
Pozzolanic Activity Index (%)	28 Days	87.8
	90 Days	97.0

Table 2.5. Chemical properties of FA.

Chemical Characteristics	**Result**
SiO_2 Soluble (%)	55.38
Al_2O_3 (%)	25.50
Fe_2O_3 (%)	6.14
CaO (%)	2.02
MgO (%)	2
SO_3 (%)	0.14
Na_2O (%)	0.62
K_2O (%)	3.8
Others	6.41

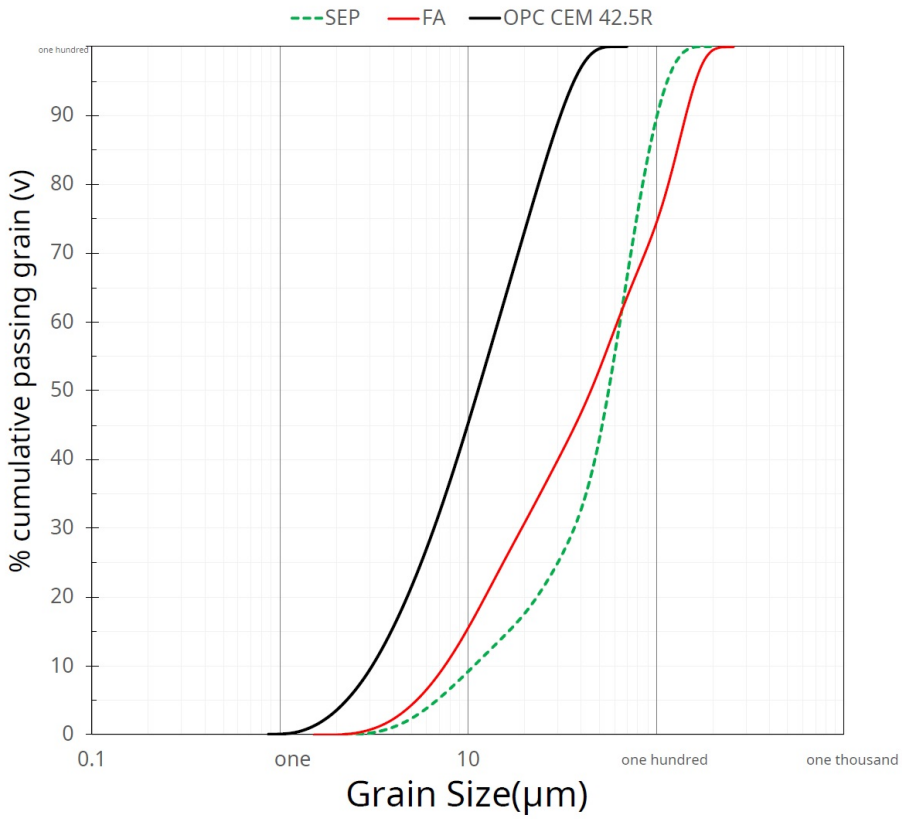

Figure 2.1. Cement (OPC-CEM 42.5R), FA-SEP particle size distribution.

2.1.3. Aggregates

Mortar samples were prepared by combining two different sizes of the silica sand AFS 10-15 (0.5-1 mm) and AFS 60-70 (0.075- 0.5mm) at a weight ratio of 2:1. AFS is a standard parameter to express the Average Fineness Size of the sands. The binder-sand ratio was kept at 1:1.5. Two different sizes of aggregates were used in this study. Due to the nozzle size of the printing robot and caulking gun, the maximum size of the sand is limited to 2 mm in diameter. Figure 2.2 displays the cumulative percent passing of the aggregate.

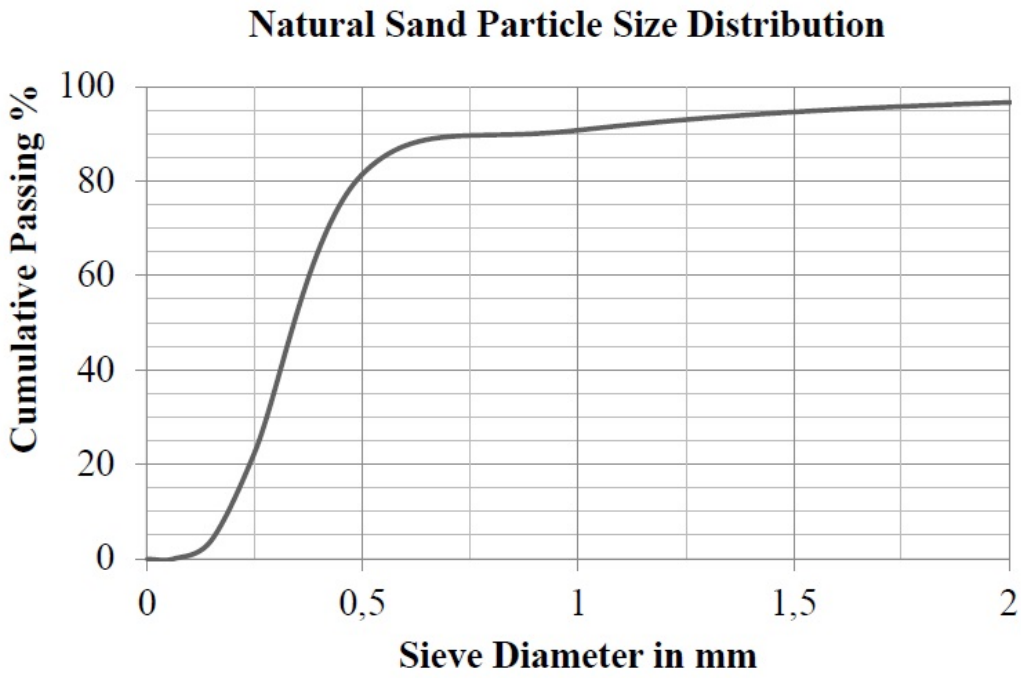

Figure 2.2. Cumulative percent passing of the aggregate.

2.1.4. Clay

Two types of nano-scale natural clay pozzolans in powder form were used as viscosity modifying agents (VMA) which contribute to shape stability by improving the thixotropic behavior of the mortar [41]. Moreover, it has been found that inserting nano clay is necessary for a successful extrusion [9]. As the first clay, NM supplied by Sigma-Aldrich with a maximum particle size of 20 µm and specific surface area of about 220 $\sim$ 270 m2/g, and as the second nano clay, SEP supplied by a local distributor ground in 150 µm were used. NM and SEP dosages were kept at 0.5% to 1% by weight of the binder.

NM as a surface-modified mineral improves the rheology of the fresh mortar by increasing the yield stress and viscosity of the material and enhances the flocculation of the material and packing density by holding some part of the mixing water [30]. Moreover, it interacts with water and improves thixotropic properties [42].

SEP is a magnesium-containing fibrous clay that not only interacts with water but also provides microstructural locking thanks to the clays it contains [43]. SEP particle size distribution was given in Figure 2.1, compared to the particle size distributions of cement and FA. Measurements were made with the Malvern laser diffraction particle size analyzer at Özyeğin University [30].

2.1.5. Plasticizer Admixture

A PCE-based SP from Sika was used at 1%-1.5% by weight of the binder to extend slump retention. It was necessary for the optimization of mix designs with considerable water reduction power [44].

2.1.6. Fiber

6 and 12 mm PA microfibers obtained from KORDSA Co. were used to provide flexural strength and stability. Fiber was added at different dosages (by weight of binder amount) to investigate the effects of the fibers on flowability and obtain the optimum amount. Table 2.6 summarizes the physical and mechanical properties of fibers.

Table 2.6. Properties of PA microfibers.

Characteristics	**Result**
Fiber Class	EN 14889-2 Class I
Density (gr/cm3)	1.38
Length (mm)	6 & 12
Filament Diameter (micron)	17-21
Tensile Stress (MPa)	800 -1100
Resistance to Corrosion	High
Melting Point [^{o}C]	255-265
Number of Fibers / Kg	200 Million
Fiber Type	Monofilament

2.2. Mixture Design

2.2.1. Preparation of the Mixes

5 different mix designs were prepared with a 0.36 water-to-binder (w/b) ratio and 20% of cement was replaced by FA as it is summarized in Table 2.7.

Table 2.7. Mix Designs (%).

Name of the mixture	**Binder**				**SP**
	Cement	FA	NM	SEP	
CONTROL	100	-	-	-	1.05
CONTROL_FA	80	20	-	-	1.05
NM_1_FA	79	20	1	-	1.05
SEP_0.5_FA	79.5	20	-	0.5	1.5
SEP_1_FA	79	20	-	1	1.5

Mix designs were prepared according to ASTM C305-20 [45] by means of an electrically driven mechanical mixer connected to a paddle, able to provide two controlled speeds.

Before starting the mixing, nano clay was mixed with SP and water for 30 seconds at 800 rpm using a magnetic stirrer until a homogenized mixture is obtained. Fiber is added by two different methods. For mixtures containing low dosages of fiber, fiber was added to the liquid part, and mixed with water and SP together. But for the mix designs containing a higher dosage of fiber, fiber was added directly to the binder and mixed with dry ingredients for 1 min separately before adding the liquid part. The reason for presuming two different mixing methodologies is that higher dosages of fibers are prone to clogging during mixing by the magnetic stirrer. Scraping time is extended from 15 s to 45 s to ensure cement particles are well scraped from the bottom of the bowl. The final mixing step also is increased from 1 min to 2 min to obtain a homogenized mixture.

2.3. Experimental Methods

2.3.1. Printing Equipment

Depending on the type of the test, two different printing setups were used in this study. The first one was a ram extruder connected to a robotic arm with an injector-type print head, available at Ozyegin University, illustrated in Figure 2.3(a). The printing process was operated at a constant speed of 13 mm/sec by the KR 6 r900 robot from KUKA, connected to a ram extruder with the 24x24 mm square nozzle shape. The second printing equipment was a special caulking gun and two rectangular nozzles with different sizes, shown in Figure 2.3(b) utilized for manual printing [34], purchased from GIVBRO. Choosing and deciding on the printing equipment for conducting each of the experiments mainly depended on the sensitivity of the test, required section shape, and test requirements. Sometimes based on the requirements and desired properties, the caulking gun showed better performance and correspondence with the requirements of the study. A variety of nozzle types are normally used in the industry including square, round, and rectangular shapes, but the rectangular shape utilized is based on the type of the experiments in the scope of this study.

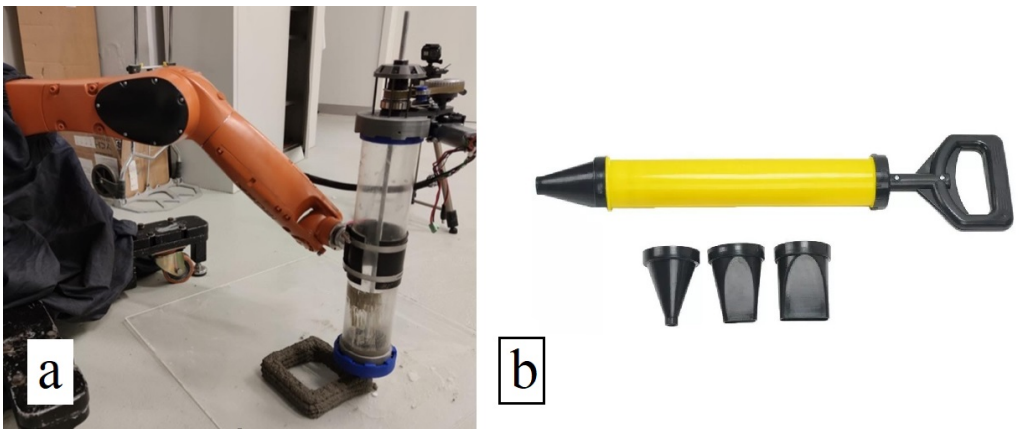

Figure 2.3. Printing setup, (a) the robotic arm and ram extruder, (b) caulking gun.

2.3.2. Preliminary Tests

2.3.2.1. Fiber Distribution. One of the critical issues and main goals of this study was to distribute PA microfibers evenly in designed mixtures. Since normally PA fiber exhibits a regular and even distribution in concrete [46], its dispersion is not critical. Considering this issue the simple visual control method [47] was employed to evaluate the distribution of the fiber in the matrix in both dry mix and hardened state. For this purpose, PA fibers were mixed with cement and FA combination in a dry mix state for 1 min and then the obtained powder mix was spread on the flat surface and divided into small parts to check the fiber content visually, shown in Figure 2.4(a). Then, another dry mixed prepared, and the fiber dispersed as it is explained for the dry mix state, and water was added to prepare fiber-reinforced mortar according to ASTM C305-20 for conducting the hardened state method. The wet mortar spread on the even smooth surface in a very thin thickness and let it dry. Finally, dried thin cement-based sheets were crushed into small pieces by using a hummer, displayed in Figure 2.4(b). Broken parts were evaluated visually after taking macro pictures to investigate the distribution of the fibers. If the fibers were present in all around the broken pieces and their distribution rate appeared to be consistent throughout the matrix, the distribution technique was deemed acceptable for the subsequent of the experiments.

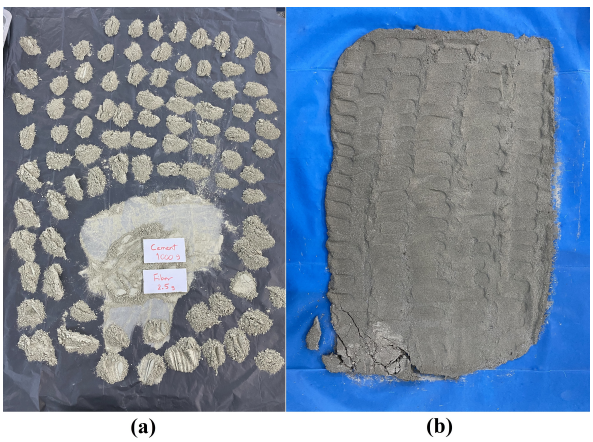

Figure 2.4. Sample preparation for fiber distribution test in, (a) dry mix, (b) hardened state.

2.3.2.2. Extrudability. This test was performed using robotic printing facilities to ensure design mortars will not clog the and will be printed smoothly. Moreover, both 6 and 12 mm fibers dispersed inside the mortar separately to evaluate their impact on extrusion to determine the fiber length for the rest of the experiments. The extrudability was evaluated by a qualitative extrusion test which focuses on defects of printed filaments. The test shape was designed as it is shown in Figure 2.5 to represent the typical way of building freeform construction components. Results were evaluated based on YES or NO. If the mortar is extruded without any blockage and fracture is not observed in the entire length of the printed filament, the mix design together with the associated fiber in that mix design is considered extrudable [24, 48].

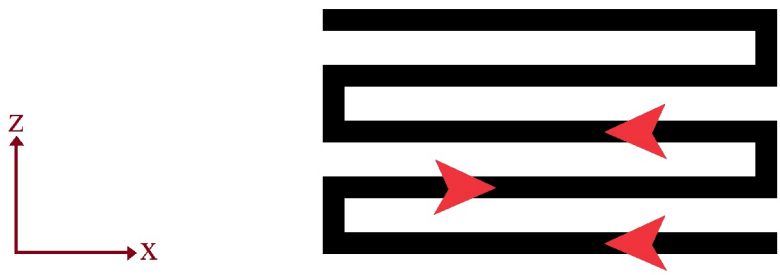

Figure 2.5. The schematic view of the process flow used for extrudability.

2.3.3. Fresh State Tests

2.3.3.1. Flowability Test. The workability characteristic of the fiber-reinforced and non-reinforced mortars was evaluated by conducting a flow table test according to the ASTM C230/230M-21 standard [49] to obtain the workable range of the mix designs. All mix designs were repeated for various dosages of fibers at the rate of 0%, 0.05%, 0.125%, and 0.150% (by weight of binder amount) to investigate the impact of fiber content on flowability, determine the optimum fiber content for the rest of the experiments and study slump loss trend. Higher fiber contents larger than 0.15% were not studied, since susceptibility for clogging and discontinuity of filaments during printing is increasing in higher contents [22].

The flowability of the mortars was evaluated by measuring the spread diameters and calculating the average diameter after conducting the flow table test over 0, 30, 60, 90, and 120 min time intervals. The test was repeated three times for each batch. The final flow diameter for each time interval was recorded as an average value from these three samples. Figure 2.6 represents the flow table test for the control mix before (a) and after (b) conducting the test.

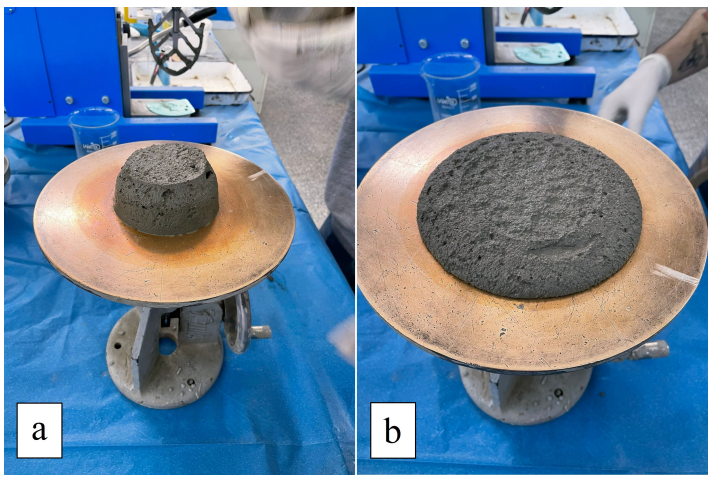

Figure 2.6. Control mix, (a) Before, (b) after the flow table test.

2.3.3.2. Buildability/Stability Test. Buildability (shape retention characteristics) as a degree of deformation attributes to the ability of printed cementitious mortar to keep its shape after extrusion against its own weight and pressure of subsequent layers [50]. For this purpose, hollow square-shaped structure printed [51] layer by layer in 5 layers in 100x100 mm dimension, displayed in Figure 2.7(a). The thickness of the layer was adjusted to 15mm by defining the printing height which is the height of the nozzle from the printing platform. The process flow of the printed geometry is schematically shown in Figure 2.7(b). Samples were printed by robotic arm using a 10x10 mm square shape nozzle at a constant printing speed of 13 mm/s.

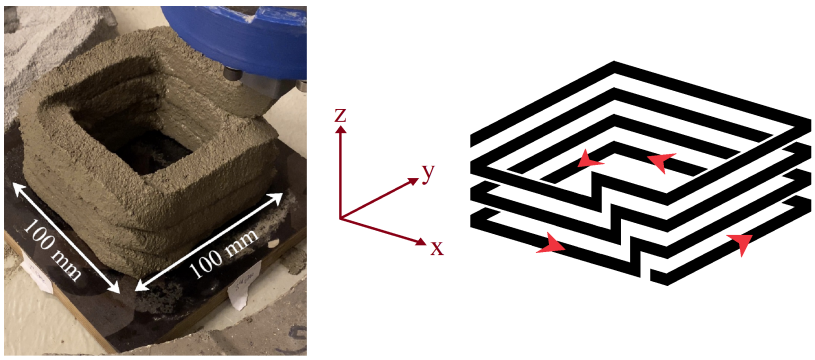

(a) **(b)**

Figure 2.7. Buildability test setup, (a) geometry and dimension of the printed hollow cube for buildability test, (b) printing path.

To evaluate the buildability, all 5 mix designs were printed accordingly. The buildability is evaluated by measuring the height of the layers on 4 sides of the printed cube (Figure 2.8) and calculating the height drop of the layers immediately after finishing the printing [52]. The measurements are repeated in different time intervals to record the changes until the moment height changes are stopped. Geometric stability is expressed as a % change in height.

Figure 2.8. Measuring the height of the printed specimen for stability test.

2.3.4. Hardened State Tests

2.3.4.1. Compressive Strength Test. To evaluate the compressive strength of the mix designs, 4-layer beams with 200 mm length were printed with a layer height of 10 mm using the caulking gun equipped with the rectangular-shaped nozzle [34], displayed in Figure 2.9(a). Nozzle output was 35 mm wide and 12 mm high, but after extrusion and as a result of the pressure of the subsequent layers, the fresh layer height dropped to 10 mm and section width increased to 40 mm. The printing process was conducted in two different manners separately with 5 and 30-minute time intervals between the layers to investigate the time gap effect on the compressive strength of the printed samples. Then, cube samples with dimensions equal to 40±2 mm were obtained by cutting the beams during the fresh state, shown in Figure 2.9(b). All samples were cured at room temperature, 22^{o}C, and 95% relative humidity until the test day. The compressive strength test of the specimens was made with a 3000 KN Automatic Compression Tester according to ASTM C 109/C109M-21 [53] and the loading rate was kept at 1±0.1 KN/s. Compressive strength was determined at 7 and 28 days after printing by loading the samples perpendicular to the printing direction. Before conducting the compression test, the upper surface of the samples was leveled by grinding using the automatic grinding machine to obtain a smooth leveled surface (Figure 2.9(c)). The compressive strength of each different mortar was determined from three samples. Finally, the results were compared to traditionally cast samples to investigate the printing effect on the compressive strength of the cementitious mortar.

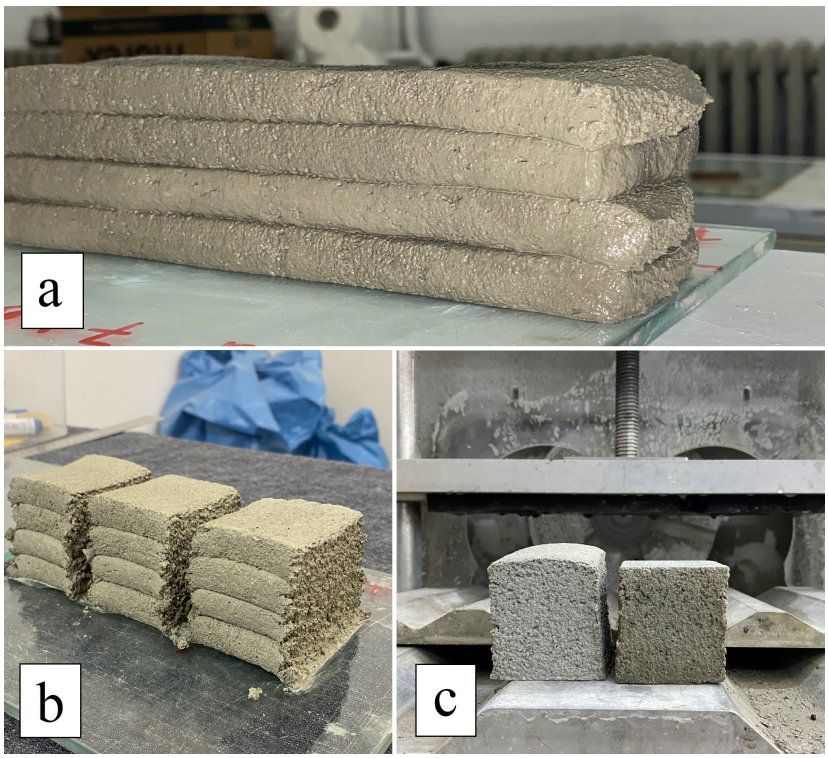

Figure 2.9. Sample preparation steps for compression test, (a) printing, (b) cutting, (c) grinding.

2.3.4.2. Interlayer Bonding Strength Test. To study the interlayer bond strength different approaches were examined and finally, two practical methods were chosen to implement. As a preliminary solution, dog-bone-shaped specimens were used and tested under uniaxial direct tensile loading [54]. For this purpose, samples were cast into a dog-bone-shaped mold at a time interval of 30 minutes. The dog-bone-shaped sample's dimension is illustrated at Figure 2.10(a). To form an interface between two parts (for imitating the interface between the printed layers), before the casting, half of the mold was separated from the middle by using a thin sheet of acetate paper as a divider to simulate interlayer formation, shown at Figure 2.10(b). Then the second half was cast after 30 min and the thin spacer was immediately removed to connect the two parts of the cast sample. The samples were removed from the mold after 24 hours and kept in the curing chamber for another 6 days at a constant temperature of 22^{o}C and 95% relative humidity until the test day. 7 days after casting, direct tensile test was performed on the samples with a servo-hydraulic closed-loop MTS test system at a loading

speed of 0.005 mm/s (Figure 2.10(c)). Alignment of the specimen in the machine was carefully done to avoid any eccentricity. The final recorded tensile load was divided by the cross-sectional area to calculate the interlayer bond strength. Three samples were prepared for each mix design.

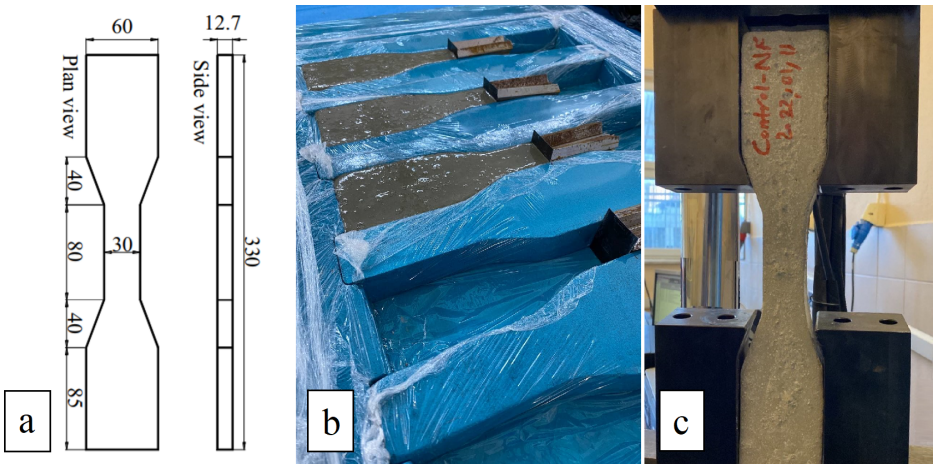

Figure 2.10. Preparing samples for direct tensile test, (a) dog-bone-shaped sample geometry, (b) forming interface using a separator, (c) conducting direct tensile test.

As the second method [55], 2-layer beams with a 30 min time interval were printed in the horizontal direction using the caulking gun equipped with the smaller rectangular-shaped nozzle. Nozzle output was 56 mm wide and 10 mm high. For each mix design, two beams (Set A and Set B) were printed. To improve interlayer bonding, cement paste was applied smoothly on the surface of the first layer of Set B (Figure 2.11) just 15 min after printing utilizing a simple brush [56, 57]. The fresh cement paste was prepared by mixing cement and water with a w/c ratio of 0.36. After another 15 min, the second layer was applied on both beams A and B to complete printing, as shown in Figure 2.11(a) and Figure 2.11(b). The schematic view of the printing steps and the whole procedure is illustrated in Figure 2.11(c).

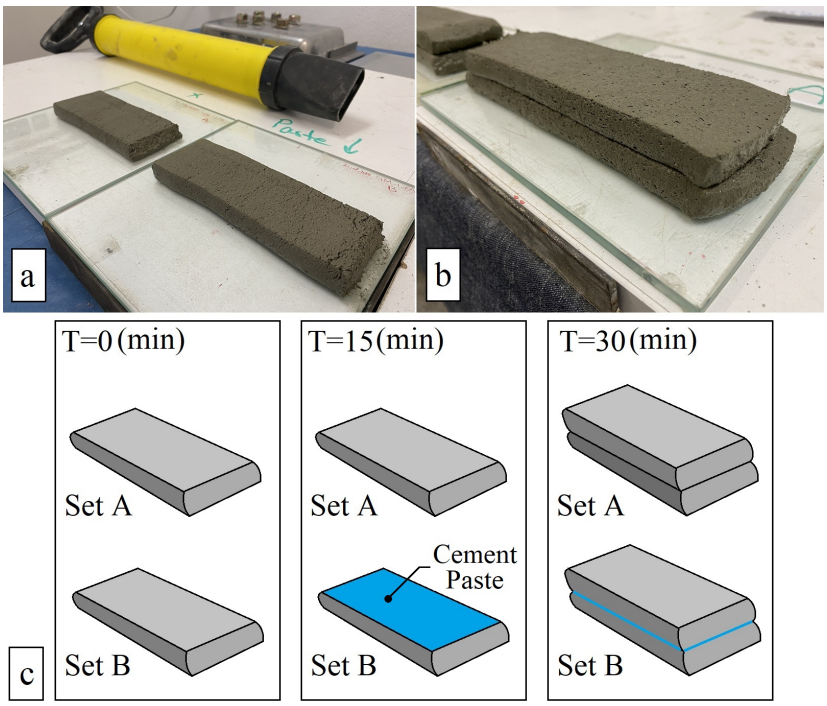

Figure 2.11. Preparing samples for interlayer bonding test, (a) printing the 1^{st} layer, (b) printing the 2^{nd} layer, (c) a schematic view of the total procedure.

One hour later, both beams were cut vertically in the fresh state using a thin steel plate [55] to obtain samples with dimensions equal to 30x30 mm and 20mm height, as displayed in Figure 2.13. All samples were cured at room temperature, 22^{o}C, and 95% relative humidity until the test day. Based on the preliminary trials, the samples obtained by this method consisting of 2 layers with a 30 min time interval showed a low bonding in a way that the 2 layers were separated during preparation (while gluing and handling) even before conducting the direct tensile test.

The weak bonding between the layers occurs due to the existence of large voids in interlayers with different intensities [34] which leads to an increased heterogeneity and systematic error in the results [58]. In the real case, the pressure of further layers improves the bonding between the layers by 10-30% [57], but in this case, just two layers exist which does not guarantee perfect bonding in the interlayer section. To tackle this problem, small pieces of steel in 40x40 mm dimension were provided and a steel nut was welded on top of it. The size of the nut was chosen in a way to provide

46g of weight (the nut and steel sheet) that is equal to the weight of 2 layers of printed specimen in size of 30x30 mm to simulate the pressure of two more layers on the printed specimen. The plate and nut structure was put on the samples immediately after cutting them to act as a uniform weight equal to the pressure of two more layers on top of the specimens, as shown in Figure 2.12.

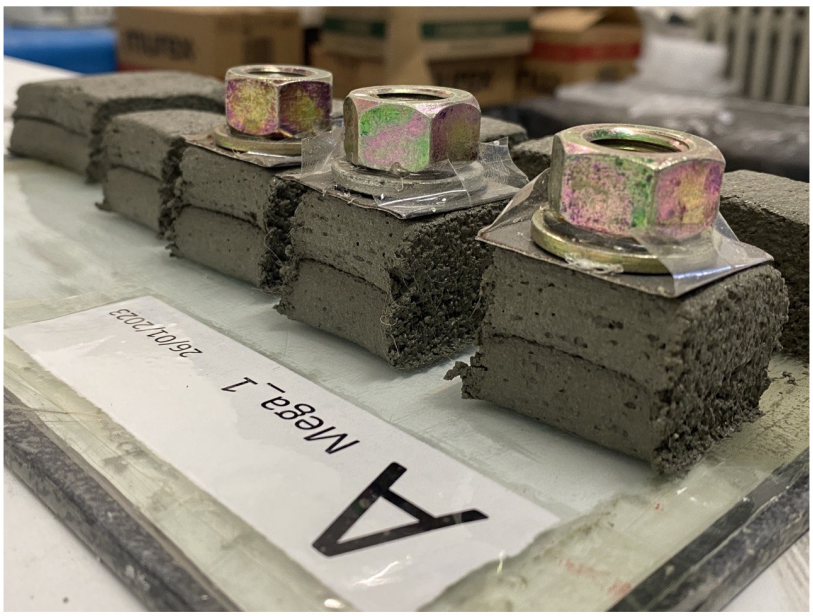

Figure 2.12. Loading additional weight on top of the samples of interlayer bonding test.

To study the failure pattern and distinguish the failure section after conducting the tensile test and before the application of the second layer, 6g of universal acrylic pigment was added to the mixture to change the second layer color (Figure 2.13) [55]. This modification was intended to facilitate the differentiation of layers during the debonding process. However, it was decided to abandon this approach after conducting preliminary trial tests, as all the samples consistently separated from the interlayer. Consequently, there was no longer a need to utilize color as the separation section could be reliably predicted.

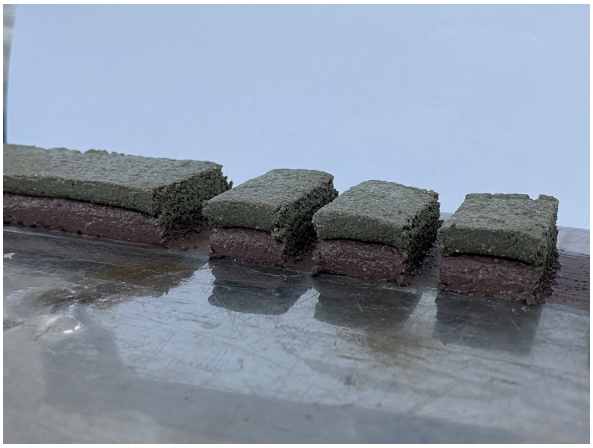

Figure 2.13. Utilizing pigment in one layer.

Then, 3 hours after printing, samples were put inside the chamber and kept at room temperature, 22^{o}C, and 95% relative humidity until the 6th day. Samples were taken out 1 day earlier to lose humidity and become dry. Since there were many specimens to test in this step, a simple test setup was designed to easily test the specimens. Two-layer cubic specimens were glued to cement-based dog-bone-shaped parts to easily remove the sample from MTS after conducting the test. A two-component epoxy-based adhesive (Figure 2.14(a)) was utilized to glue dog-bone-shaped samples to the two sides of the samples [55, 56], shown in Figure 2.14(b). The schematic view of the prepared sample setup is displayed in Figure 2.14(c).

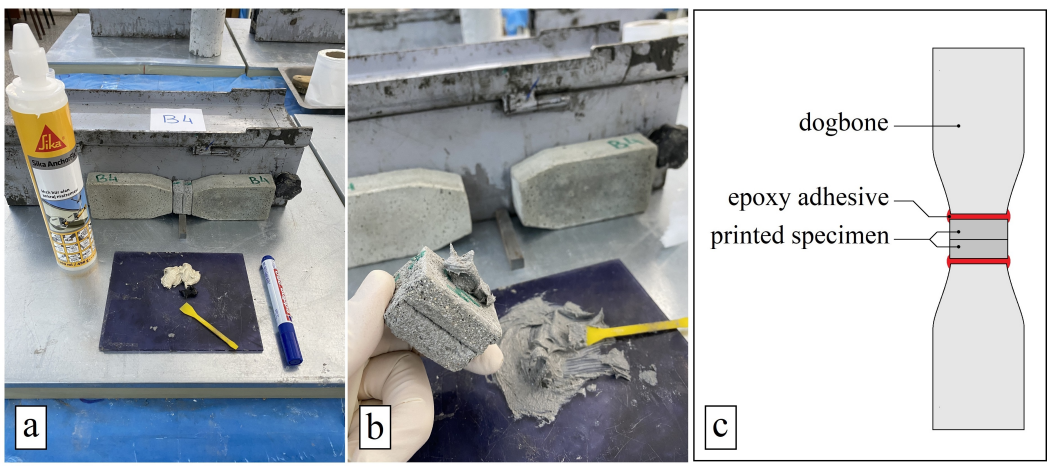

Figure 2.14. Preparing samples for the MTS test, (a) preparing adhesive, (b) gluing, (c) a schematic view of the specimen.

Finally, uniaxial tension (Figure 2.15(a)) was applied to the samples by using an MTS machine at the rate of 0.005 mm/sec [59] as it is shown in Figure 2.15(b). Totally 6 specimens were produced for each mix design including 3 specimens for set A and 3 more specimens for set B whose interlayer bonding was improved by applying a cement paste layer (Figure 2.15(c)). Moreover, the control mix design was repeated once again with a 0 min time delay to investigate the delay effect on interlayer bonding strength.

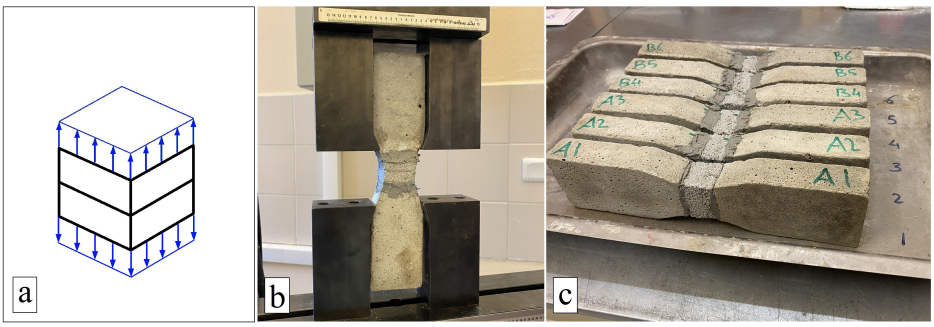

Figure 2.15. Direct tensile test setup, (a) uniaxial tensile loading direction, (b) tensile bond strength setup, (c) A and B series ready for the test.

After the test, photos were taken from the separated sections of all specimens one by one to determine the failure pattern and calculate the effective area. The effective area was obtained after analyzing the failure section and calculating the area in ImageJ software, as shown in Figure 2.16. The bonding strength was calculated based on the maximum failure load obtained from MTS and the effective bonding area derived from image analysis [60].

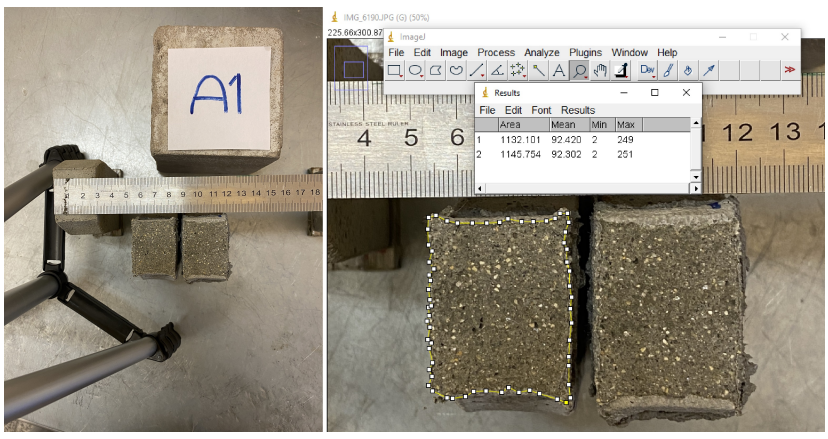

Figure 2.16. Section analysis after failure by Image J software.

2.3.4.3. Flexural Strength Test. To investigate the flexural strength characteristic, samples were prepared by both casting and printing methods separately. Casting method aimed to check the fiber content effect on flexural properties. For this purpose, 40x40x160 mm prisms were cast manually and a 3-point bending test was conducted with a servo-hydraulic displacement-controlled device according to the ASTM C348 standard [61] for the three-point bending test of mortar prisms. The free span length was adjusted at 100 mm and the loading rate was set to 50 N/s.

Then, samples were printed for equal content of fiber (0.15%) to compare the flexural properties of different mix designs. 2-layer beams were printed continuously in the horizontal direction [34] in 160 mm length using the robotic arm and ram extruder at a constant printing speed of 13 mm/s. The flow path is shown in Figure 2.17(a) and the specimen geometry and loading configuration is shown in Figure 2.17(b). 3 specimens were printed for each mix design on the oiled wooden platform as it is displayed in Figure 2.17(c). The square shape nozzle was utilized for the experiment with 24x24 mm output and the thickness of the layers was adjusted to 15mm by defining the nozzle distance from the printing surface. 3 hours after printing, samples were transferred to a climatic chamber and kept at room temperature, 22^{o}C, and 95% relative humidity until the test day. Finally, a 3-point bending test was conducted with a servo-hydraulic displacement-controlled device on the 28th day (Figure 2.18). Maximum stress was recorded and divided by the section area to calculate the flexural strength of the prisms.

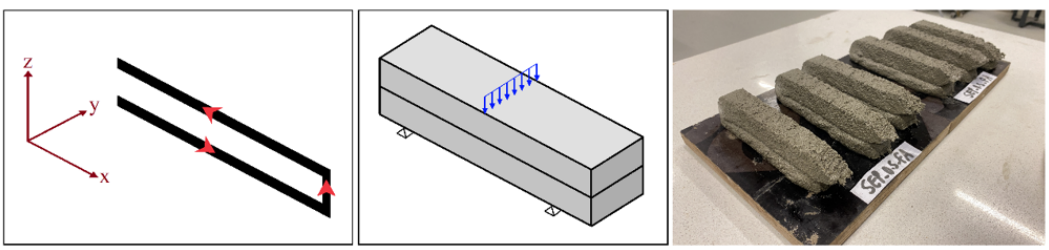

Figure 2.17. 3-Point bending specimens, (a) the flow path, (b) loading configuration (c) printed prisms.

Figure 2.18. 3-Point bending test setup.

3. RESULTS AND DISCUSSION

3.1. Preliminary Test Results

3.1.1. Fiber Distribution

Fibers were supposed to be dispersed at the rate of 0%, 0.05%, 0.125%, and 0.150% (by weight of binder amount) inside the water of the mixtures using a magnetic stirrer until obtaining a homogenized mixture. 0.05% and 0.125% fiber contents were mixed properly by this technique, but when fiber content increased to 0.150%, the magnetic stirring bar clogged between high-volume fiber content, and the mixing action was interrupted. This problem intensified in mixed designs which contain clay inside, since by the addition of clay, the density of the mixture increased and clay dispersion action also was interrupted. Moreover, fibers agglomerated and clumped in one point of the water as it is shown in Figure 3.1, which in this case, it becomes very difficult to remix and disperse them.

Figure 3.1. Fiber clump problem in 0.15% volume.

To disperse fibers in higher content (0.15%) for mix designs which include clay, other methods were investigated. The best result was obtained when fibers were mixed inside a dry mix of cement using a mechanical mixer at a lower speed for one minute.

Fiber dispersion analysis was done by processing 2D digital images and visual analysis. In the first step, PA fibers were distributed in a dry mix of binder by mixing, and the obtained mixture spread on the flat surface as it was explained before. After evaluating all parts of the dry mix with the naked eye, it was proven that distributing PA fibers by a 1-min dry mix with binder was an efficient method for high contents (0,15%) and 1 min is enough time to ensure all fiber content is distributed uniformly. As a result, 60 seconds was recorded as a preliminary mixing time for distributing PA fibers in the dry mix, before adding water and other ingredients in the mix. A photo taken from one part of the spread dry mix is shown in Figure 3.2.

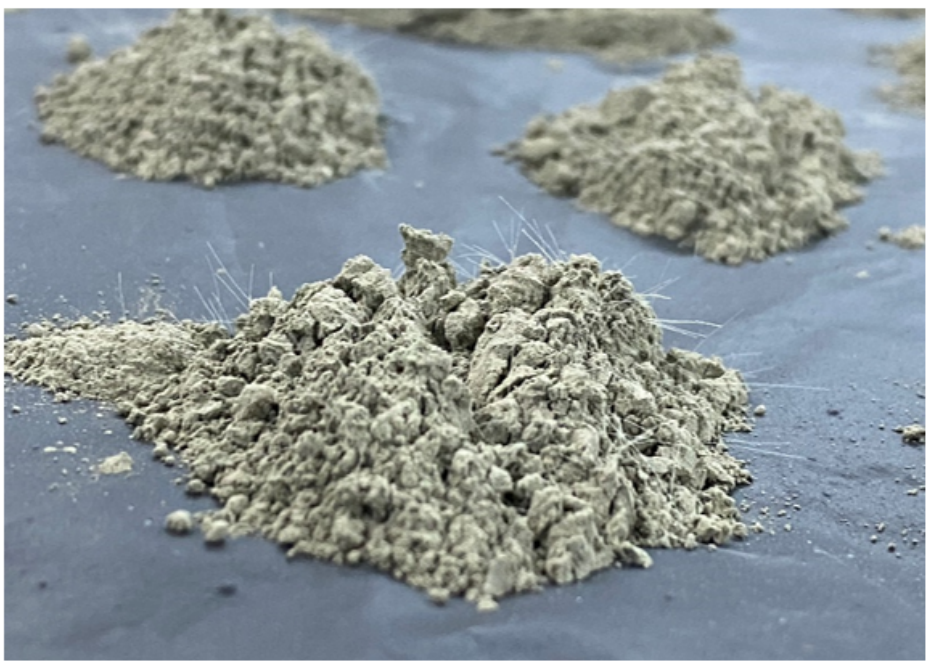

Figure 3.2. Distribution of PA fibers in dry mix.

Then, fiber distribution was evaluated for prepared mortar. A thin layer of fiber-reinforced mortar was prepared according to ASTM C305-20 and investigated after drying and crushing into small pieces. After taking pictures from all around the crushed matrix and cracks, it was seen that fibers were well distributed in the entire mortar

matrix. Figure 3.3 illustrates fiber distribution by three photos taken from 3 distinct sections of the crushed reinforced mortar with PA fibers.

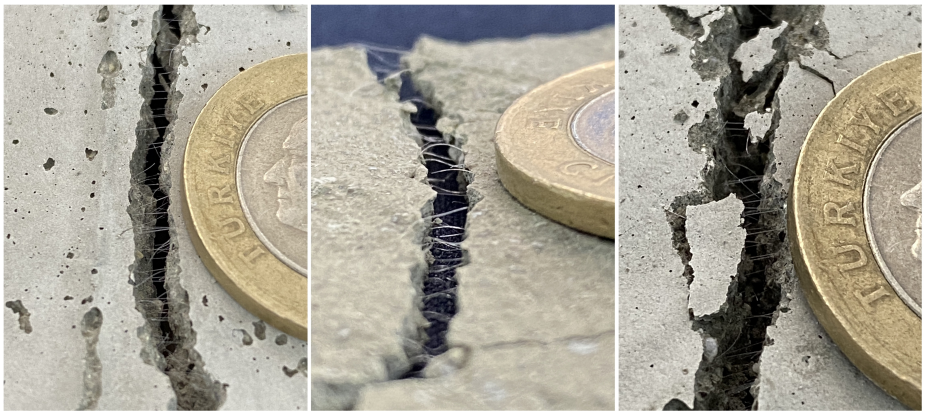

Figure 3.3. Distribution of PA fiber in crushed mortar.

3.1.2. Extrudability

To ensure design mixes are extrudable, control mixes containing 6 and 12mm fiber were printed by using the printer connected to a ram extruder using a 24x24 mm square shape nozzle at a constant printing speed of 13 mm/s. Both 6 and 12 mm fiber-containing mix designs were extruded continuously without any significant sign of fracture. Obtained results are evaluated based on YES or No for tested mix designs as it is shown in Table 3.1.

Table 3.1. Extrudability results for different fiber lengths.

Mix Design	**Fiber length (mm)**	**Extrudable**
Control	6	YES
Control	12	YES
Control-FA	6	YES
Control-FA	12	YES

Since both 6 and 12mm fiber-reinforced mortars showed the same performance in terms of distribution and extrudability, 12 mm PA fiber was chosen as the desired length for conducting the rest of the experiments.

3.2. Fresh State Test Results

3.2.1. Flowability Test Results

3.2.1.1. Determining SP Amount. The first aim of this part was to find the optimum amount of SP for mix designs. For this purpose, the CONTROL and CONTROL-FA mixes were examined separately with different amounts of SP to obtain desired flowability for each one. Based on the experience and observations from previous phases of this project, the ideal flowability as a target value for printing with the KUKA printer and associated ram extruder and the square nozzle shape with a 24x24 mm opening was expected to be 19-21cm, approximately. CONTROL mix with SP=0.35%, 0.70%, and 1.05% by weight of binder was prepared accordingly and flow table tests were conducted at t=0, 30, 60, 90, and 120 min. Obtained results are shown in Figure 3.4. It can be observed from this figure that the SP amount of 1.05%, had the most desirable flowability with the required range. The test was repeated for SEP_0.5_FA which contains SEP with SP=1.0%, 1.3%, and 1.5% by weight of binder, since SEP has high water absorption potential. Based on the obtained results shown in Figure 3.5, an SP amount of 1.5% was chosen as the optimum amount of SP for SEP-containing samples.

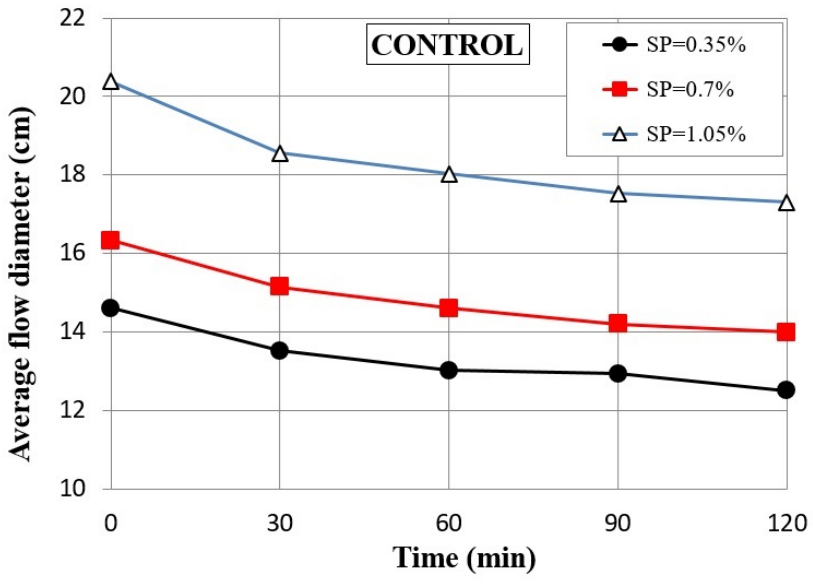

Figure 3.4. Results of flow table test for control mix with various SP amount.

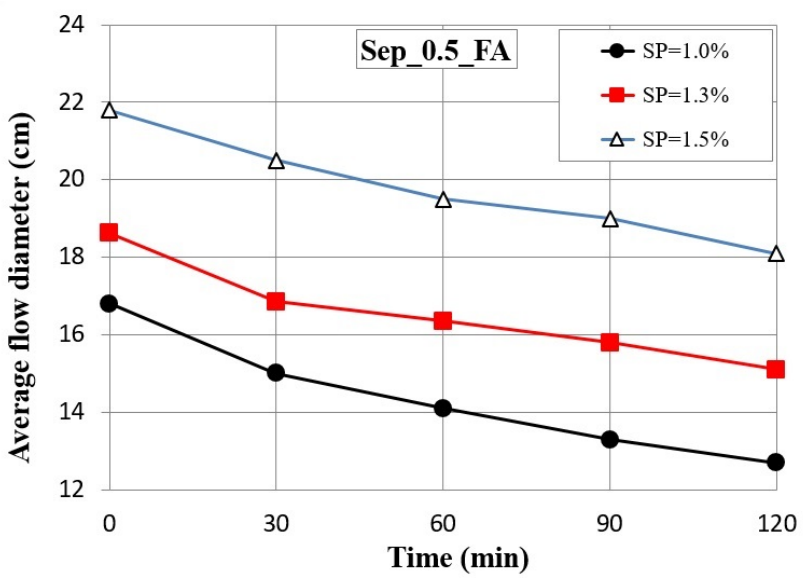

Figure 3.5. Results of flow table test for SEP_0.5_FA with various SP amount.

3.2.1.2. Evaluating flowability of non-reinforced mixtures. After determining the optimum SP amount, the flow table test was conducted for all mix designs to compare their flowability before adding fibers, as shown in Figure 3.6. As expected, the addition of FA to the samples improved the initial workability (t=0). The flowability of CONTROL-FA was improved by up to 10%, but flow loss increased considerably in the first 60 minutes after mixing the mortar by 20% replacement of cement by FA, as it is given in Table 3.2. The addition of 1% of clay (NM and SEP) in the NM_1_FA and SEP_1_FA samples significantly reduced the workability compared to their counterpart CONTROL_FA sample. However, the NM-containing sample maintained the flow better than the SEP-containing one in 2 hours based on the results in Table 3.2. Due to this potential of NM in keeping the flow, the flowability of the NM_1_FA after 2 hours exceeds the flow of its counterpart CONTROL_FA as can be seen in Figure 3.6.

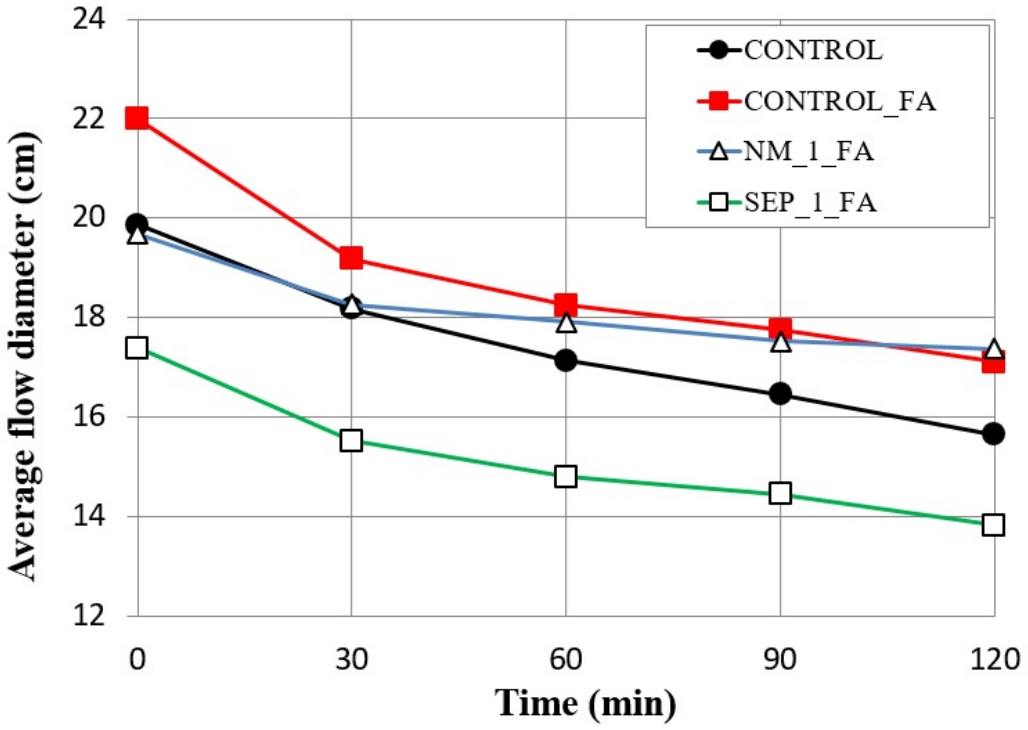

Figure 3.6. Result of flow table test for mix designs without fiber.

Table 3.2. Flow table test results for mix designs without fiber.

Mix Designs	Flow diameter (cm) at t (min) intervals					Flow Loss (%) in 60 min	Flow Loss (%) in 120 min
	t=0	t=30	t=60	t=90	t=120		
CONTROL	19.9	18.2	17.1	16.5	15.7	13.7	21.2
CONTROL_FA	22.0	19.2	18.2	17.7	17.1	17.1	22.2
NM_1_FA	19.7	18.3	17.9	17.5	17.4	9.0	11.7
SEP_1_FA	17.4	15.5	14.8	14.5	13.8	14.9	20.5

Another individual comparison was done to study and compare the effect of increasing clay content from 0.5% to 1.0% on the workability of the mortar. Based on the obtained results, increasing SEP content resulted in flow loss, ranging from 23.2% to 26.8% for different time intervals in a 2-hour period. On the other hand, increasing NM content resulted in a slight flow loss ranging from 4% to 10.8% in the

same period. Evaluating the results given in Table 3.3 and comparing the flowability diagram of clay-containing samples (Figure 3.7 and Figure 3.8) revealed that increasing SEP content significantly decreased workability while increasing NM content by the same amount resulted in a slight decrease in the workability of the samples. These results demonstrate NM's influence on flow loss is considerably less than SEP. Although both NM and SEP as nanomaterials have high specific surface areas to interact with water, due to the hydrophilic properties of SEP, it absorbs higher water content, and that is why SEP-containing samples lost workability more than NM containing samples over time [62].

Table 3.3. Flow table test results for NM and SEP containing Mixtures.

Sample	**Flow diameter (cm) at t (min) intervals**				
	t=0	**t=30**	**t=60**	**t=90**	**t=120**
NM_0.5_FA	20.5	20.5	20.0	19.7	19.2
NM_0.5_FA	20.5	20.5	20.0	19.7	19.2
NM_1_FA	19.7	18.3	17.9	17.5	17.4
Loss %	**4.0**	**10.7**	**10.4**	**10.8**	**9.7**
SEP_0.5_FA	22.6	21.2	20.0	19.3	18.5
SEP_1_FA	17.4	15.5	14.8	14.5	13.8
Loss %	**23.2**	**26.8**	**25.9**	**25.2**	**25.1**

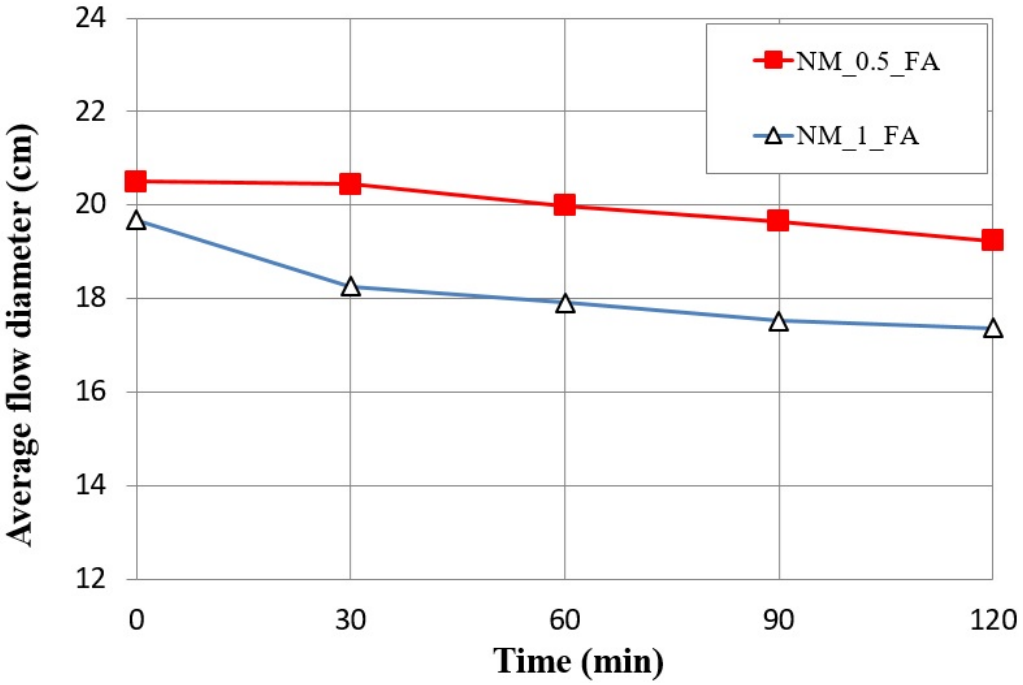

Figure 3.7. Effect of NM content on flowability.

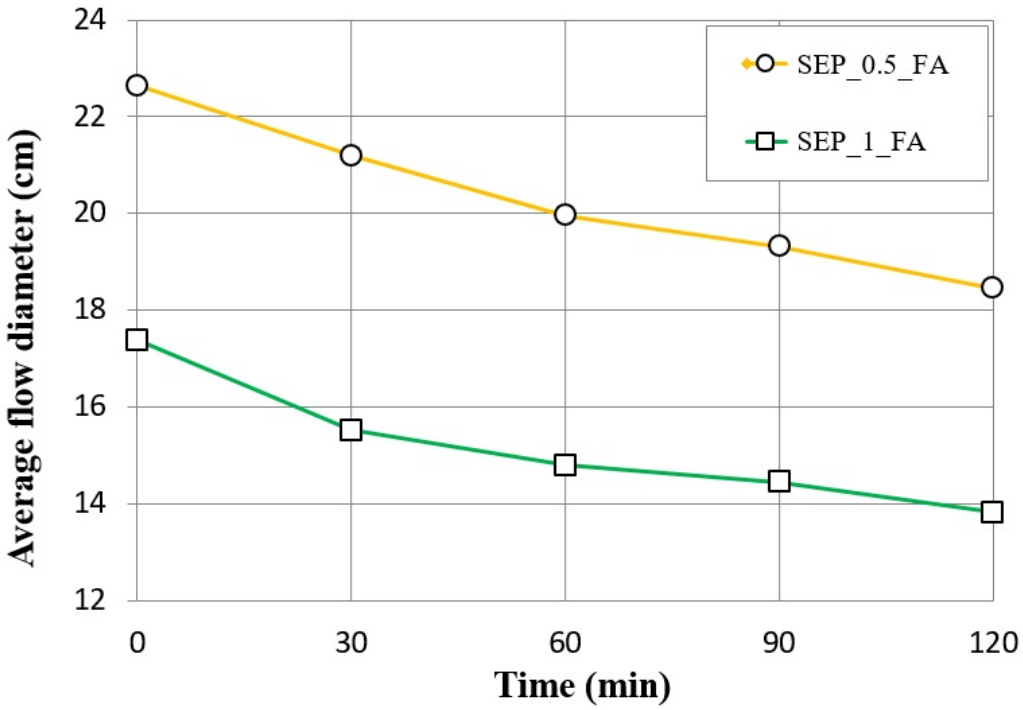

Figure 3.8. Effect of SEP content on flowability.

3.2.1.3. Evaluating flowability of fiber-reinforced mixtures. Then PA fibers were introduced to the mixtures to investigate the workable range of fiber-reinforced mortars and study workability change behavior in all mix designs for various dosages of PA fibers (0%, 0.05%, 0.125%, and 0.150%) by weight of binder amount. For beginning CONTROL and CONTROL_FA mixtures were studied by conducting flow table tests for mentioned contents of fibers accordingly. Based on the results obtained in the fiber distribution section, all fiber contents directly were mixed inside water for both CONTROL and CONTROL_FA samples as it was explained before. For both CONTROL and CONTROL-FA, workability decreased slightly with an increased PA fiber volume as it was expected, shown in Figure 3.9 and Figure 3.10, respectively.

The flowability loss in percentage is calculated for CONTROL mix after 60 and 120 min for all fiber volumes, shown in Table 3.4. Based on the obtained results for the CONTROL mix, the maximum flowability loss occurred for 0.05% and 0% fiber-reinforced samples by 14% and 13.7% (after 60 min), respectively. In the same way, maximum flow loss was recorded for 0% and 0.05% fiber content samples by 21.2% and 18.7% (after 120 min), respectively. On the other hand, minimum flowability loss was observed for 0.125% and 0.150% fiber contents by 12.2% and 17.6% after 60 and 120 min, respectively. When the values given above are considered it can be said that the effect of fiber reinforcement on the flow loss was limited.

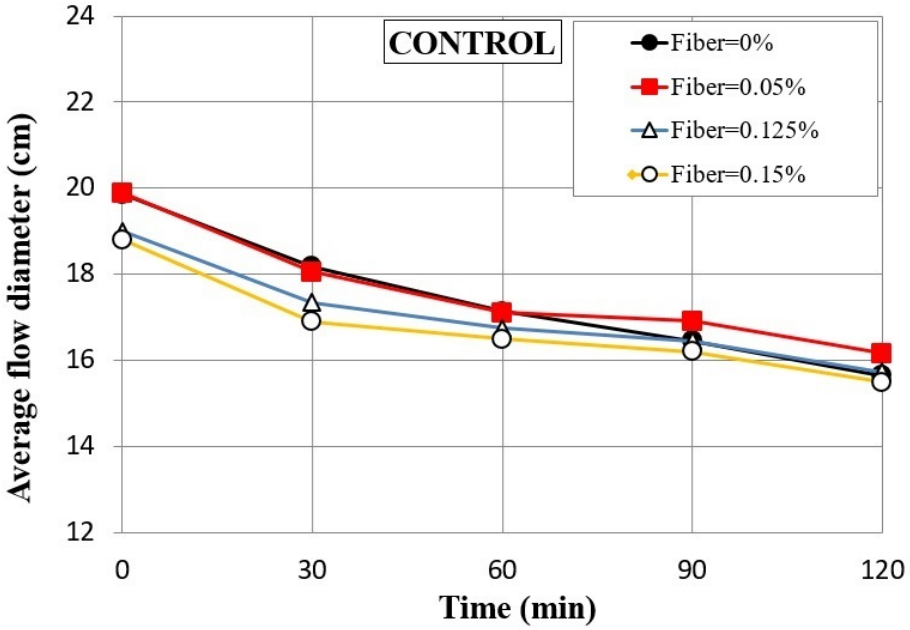

Figure 3.9. Flow table test results for CONTROL mixes containing different dosages of PA fibers.

Table 3.4. Flow table test results for CONTROL mixes containing different dosages of PA fibers.

Fiber content	**Flow diameter (cm) at t (min) intervals**					**Flow Loss (%) in 30 min**	**Flow Loss (%) in 60 min**	**Flow Loss (%) in 120 min**
	T= 0	**T= 30**	**T= 60**	**T= 90**	**T= 120**			
0%	19.9	18.2	17.1	16.5	15.7	8.5	13.7	21.2
0.05%	19.9	18.1	17.1	16.9	16.2	9	14.0	18.7
0.125%	19.0	17.3	16.7	16.5	15.6	8.9	12.2	17.5
0.15%	18.8	17.3	16.5	16.2	15.5	7.9	12.2	17.6

The flowability loss in percentage is calculated for CONTROL_FA mix after 60 and 120 min for all fiber volumes, shown in Table 3.5. Based on the obtained results for the CONTROL_FA mix, the maximum flowability loss occurred for 0% fiber (plain) sample by 17.9%, after 60 min. In the same way, maximum flowability loss was recorded

for 0% fiber content samples by 22.5%, after 120 min. On the other hand, minimum flowability loss was observed for 0.15% fiber content by 10.3% and 16.5% after 60 and 120 min, respectively.

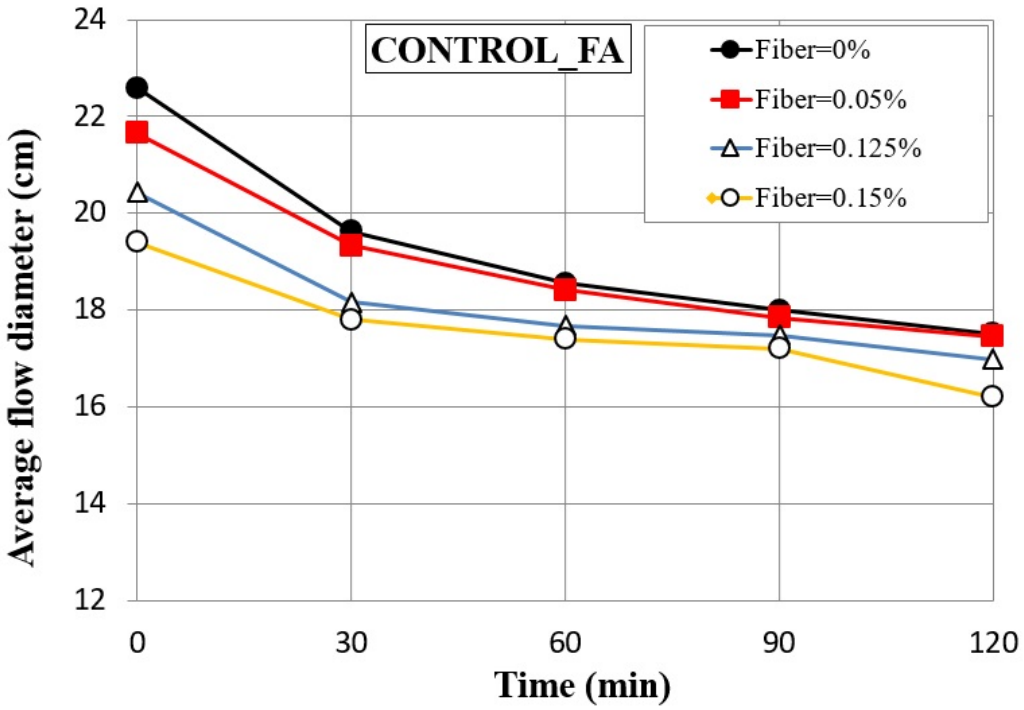

Figure 3.10. Flow table test results for CONTROL_FA mixes containing different dosages of PA fibers.

Table 3.5. Flow table test results for CONTROL_FA mix containing different dosage PA fibers.

Fiber content	**Flow diameter (cm) at t (min) intervals**					**Loss % in 30 min**	**Loss % in 60 min**	**Loss % in 120 min**
	T= 0	**T= 30**	**T= 60**	**T= 90**	**T= 120**			
0%	22.6	19.6	18.6	18.0	17.5	13.3	17.9	22.5
0.05%	21.7	19.3	18.4	17.9	17.5	11.05	15.0	19.4
0.125%	20.4	18.2	17.7	17.5	17.0	10.8	13.4	16.9
0.15%	19.4	17.8	17.4	17.2	16.2	8.24	10.3	16.5

Evaluating Table 3.4 and Table 3.5 results and comparing the flowability of the CONTROL and CONTROL_FA mixtures with and without fiber revealed that the increasing PA fiber content from 0 to 0.15%, hinders the flow loss and maintains the workability of the mortar during the whole time intervals of a 2-hours period. It might be due to the hydrophilic nature of PA fibers [63], which restore water and restricts water loss from the matrix of cement paste. But it is obvious that by increasing fiber content, the workability of the sample decreases due to the water absorption behavior of PA fiber. Moreover, the workability loss of the reinforced mortar at an initial 30 min was more intense since mixtures lost almost half of their flowability at an initial 30 min while considering the 2-hour period.

The flow diameter changes of clay-containing mixtures is shown in Figure 3.11, and their flow loss behavior is compared with their co-respondent control mix (CONTROL_FA) in Table 3.6 when 0.125% of PA fibers are added. Similar to the non-reinforced situation, the NM-containing sample maintained the flow better than SEP containing one and their co-respondent control mix, in a 2-hour period. It means the addition of 0.125% of fibers did not change the mixtures‘ flow behavior compared to the non-reinforced state. Figure 3.12 illustrates the flow table test result immediately after mixing (t=0) and 2 hours for CONTROL_FA and NM_1_FA samples.

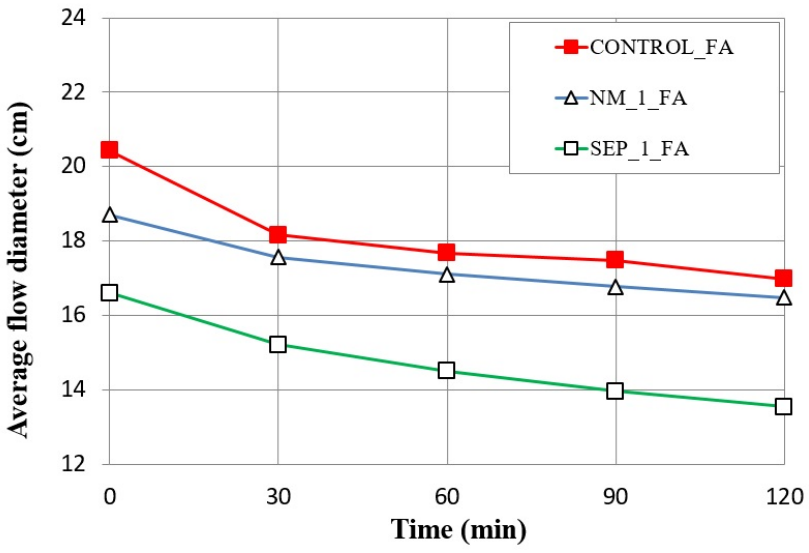

Figure 3.11. Results of flow table tests for mix designs containing 0.125% PA fiber.

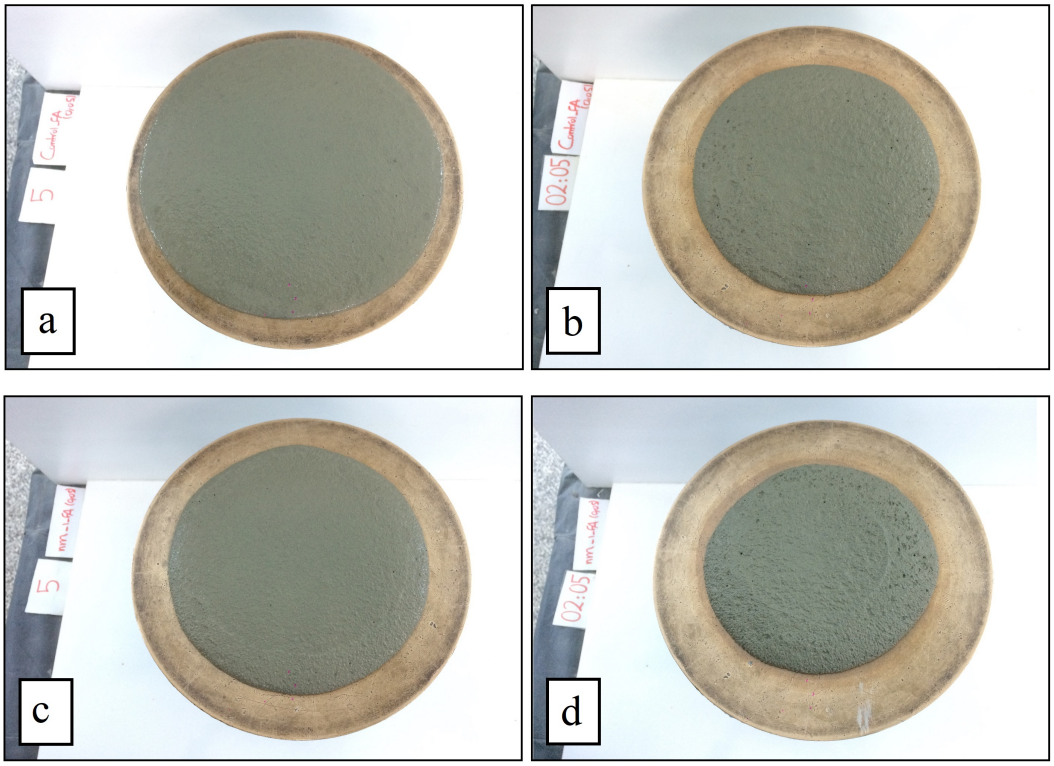

Figure 3.12. Flow Table tests conducted for CONTROL_FA at, (a) t=0, (b) t=120 min and NM_1_FA at, (c) t=0 (d) t=120 min.

Table 3.6. Flow Table test results for mix designs with 0.125% PA fiber.

Mix Designs	**Flow diameter (cm) at t (min) intervals**					**Loss % in 30 min**	**Loss % in 60 min**	**Loss % in 120 min**
	T= 0	**T= 30**	**T= 60**	**T= 90**	**T= 120**			
CONTROL_FA	20.4	18.2	17.7	17.5	17.0	11.1	13.4	16.9
NM_1_FA	18.7	17.6	17.1	16.8	16.5	6.1	8.6	11.9
SEP_1_FA	16.6	15.2	14.5	14.0	13.5	8.4	12.6	18.5

To study and observe the flow behavior of clay-containing samples against increasing fiber volume, Figure 3.13 was provided and flow loss line diagrams were prepared for a 2-hour time period. It is obvious from this figure that the addition of SEP to the mixture resulted in higher flow loss compared to NM as it was mentioned before.

Moreover, the narrow distance between line diagrams in NM_1_FA (Figure 3.13(b)), illustrates NM resistance against flow loss at all fiber volumes over a 2-hour period. But NM_1_FA considerably lost its workability in all time intervals when fiber content increased from 0.05% to 0.125% compared to SEP_1_FA which did not show significant change in its workability (except t=0) with an increase in fiber content. This issue can be seen by comparing the slope of the lines in Figure 3.13 and it is proved by presented analysis in Table 3.7. When fiber content was increased, NM-containing samples lost their workability significantly in all time intervals more than SEP-containing samples. Based on this table, immediately after mixing (t=0), both NM_1_FA and SEP-1_FA showed almost same flow loss (4.5%-5%) when 0.125% of fibers were added, but by the time, SEP containing samples could maintain the flow better with only 2% flow loss, while NM_1_FA workability reduced by 3.8%, 4.5% and 5.2% after 30, 60 and 120 min, respectively. The highest flow loss was recorded for CONTROL_FA at t=0 by 7.1% loss when fiber content was increased to 0.125%.

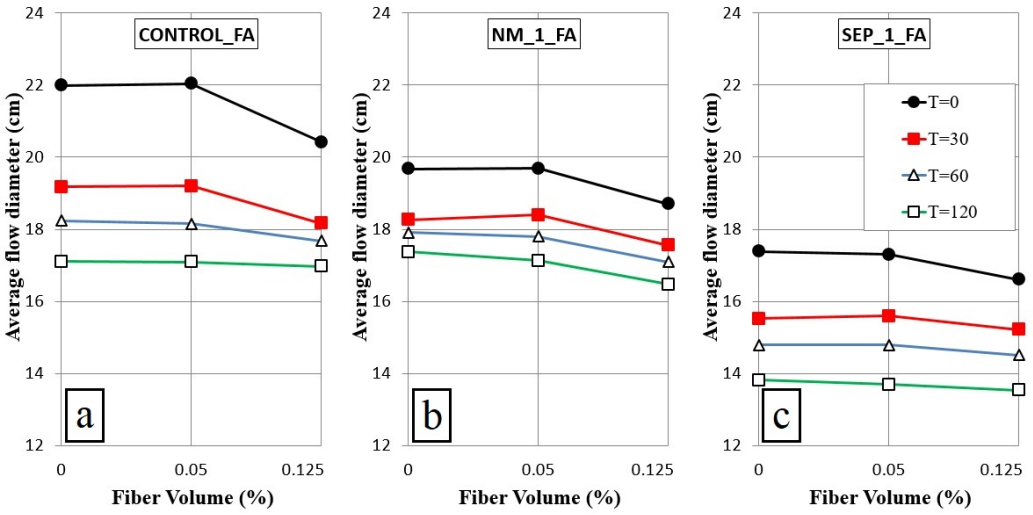

Figure 3.13. Flow loss of clay containing samples in different dosages of PA fibers in a 2-hour period, (a) CONTROL_FA, (b) NM_1_FA (c) SEP_1_FA.

Table 3.7. Flow loss of clay containing samples in different dosages of PA fibers in a 2-hour period.

Mix Designs	**Fiber Volume (%)**	**Flow diameter (cm) at t (min) intervals**			
		T=0	**T=30**	**T=60**	**T=120**
CONTROL_FA	**0**	22.0	19.2	18.2	17.1
	0.05	22.0	19.2	18.2	17.1
	0.125	20.4	18.2	17.7	17.0
	Loss % for 0.125%	7.1	5.3	3.1	0.8
NM_1_FA	**0**	19.7	18.3	17.9	17.4
	0.05	19.7	18.4	17.8	17.1
	0.125	18.7	17.6	17.1	16.5
	Loss % for 0.125%	5.0	3.8	4.5	5.2
SEP_1_FA	**0**	17.4	15.5	14.8	13.8
	0.05	17.3	15.6	14.8	13.7
	0.125	16.6	15.2	14.5	13.5
	Loss % for 0.125%	4.5	2.0	2.0	2.0

To conclude, the influence of NM on the workability of the cementitious mortar is much less than SEP. This can be attributed to the hydrophilic nature of SEP which induces a higher water retention and absorbs the excess water of the mortar [64]. Therefore, when PA fiber as a hydrophilic fiber is added to the SEP-containing mortar, it is hypothesized that there is less excessive water to be absorbed by fibers, so workability changes slightly, but NM containing sample has more excessive water in its matrix compared to SEP containing sample and that is why when PA fibers are added, some part of the available excess water is absorbed by PA fibers and workability of NM_1_FA decreases more than SEP_1_FA in 2 hours.

3.2.2. Buildability Test Results

To evaluate the buildability, all the mix designs were printed with 0.15% fiber content using an extruder connected to a robotic arm to evaluate the shape retention potential of NM and SEP and compare the results with the CONTROL_FA mixture. Moreover, the CONTROL sample also was printed to check the effect of FA on the buildability of the mixes. The initial plan was to print a hollow square-shaped structure in 6 layers, but due to the small size of the cylinder of the extruder, there was not enough mortar to complete the 6th layer properly. As result, air entrapped in the mortar during the extrusion of the 6th layer, which caused irregularity in the shape of the section and resulted in instability and failure of the whole structure, as it is shown in Figure 3.14. That is why the experiment was conducted by printing the hollow structure in 5 layers.

Figure 3.14. Failure of the structure during printing of the 6^{th} layer.

Immediately after printing, photos were taken from all 4 sides of the structure while a ruler was placed in front of each side to measure the height of each layer and analyze the height loss in a time period. The measurement was repeated in 5, 15, 30, and 60 min time intervals, accordingly. Figure 3.15 depicts the images taken from

all samples during the buildability test 60 min after printing. It is clear from this figure that, NM_1_FA and SEP_0.5_FA inherited uniform structure and showed better cohesion which is attributed to the existence of clay in their mixtures. Moreover, the 1st layer of CONTROL_FA deformed considerably as a result of the pressure of the other deposited layers which shows the low buildability characteristics in CONTROL_FA, based on the measurements at the beginning (t=0 min), illustrated in Table 3.8.

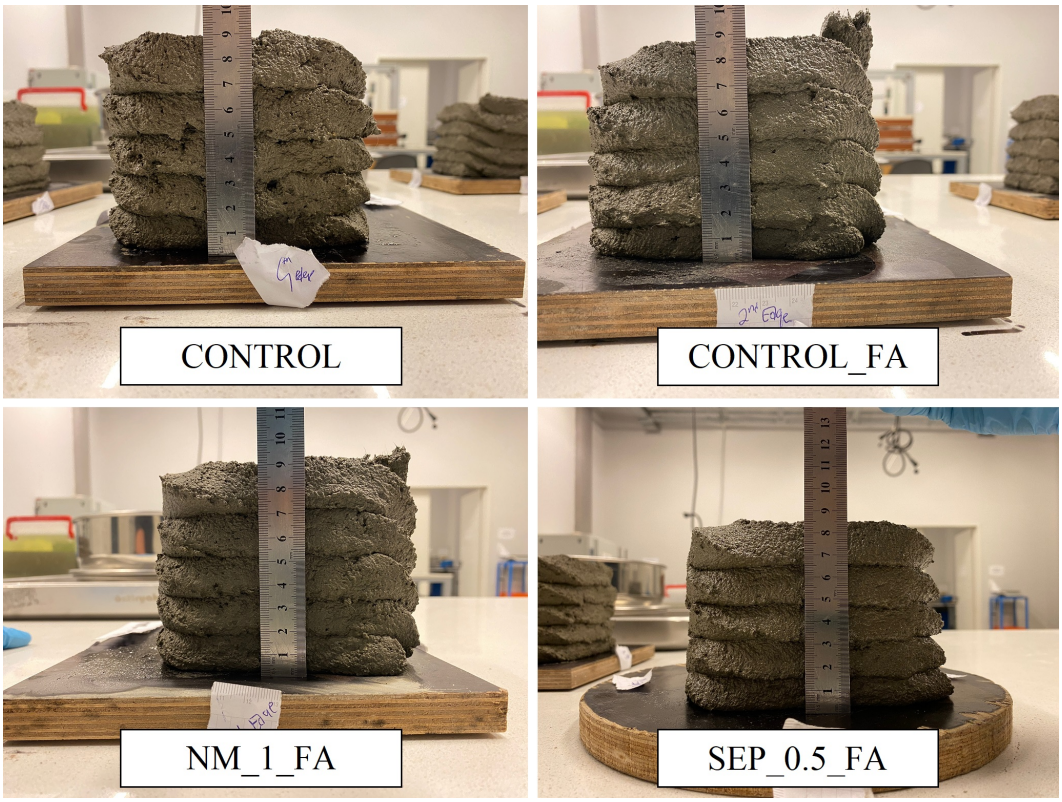

Figure 3.15. Printed samples for buildability test 2 hours after printing.

Table 3.8. The layer height of the samples immediately after printing.

Samples	**Layer Height (mm) at t=0**				
	1st	**2nd**	**3rd**	**4th**	**5th**
CONTROL (0.15%)	17	16	17	18	19
CONTROL_FA (0.15%)	8	17	18	19	18
NM_1_FA (0.15%)	17	18	19	16	21
SEP_0.5_FA (0.15%)	15	16	19	18	20

After 60 minutes, no change was detected in the height of the samples, so the experiment stopped and results were analyzed in order to compare the buildability behavior of all samples. Table 3.9 summarizes the results based on the total height as an average of the final height obtained from all sides in a 2-hour period, and Table 3.10 presents the geometric stability as a percentage change of the height in each time interval. It is obvious from Table 3.9, that NM_1_FA demonstrated the highest buildability potential among other samples by obtaining 93 mm height. The result of the buildability test also is shown in Figure 3.16, displaying the initial and final height of the structures. By comparing the results of NM_1_FA and SEP_0.5_FA with CONTROL_FA, it can be concluded that the addition of SEP and NM improved the buildability behavior of the mixtures by 3.6% and 12%, respectively. The high standard deviation for CONTROL-FA originates from unequal height of 4 sides which explains its poor behavior in maintaining its shape. When Table 3.10 was evaluated, it was seen that height loss in all of the samples stopped 15 minutes after printing. It means all samples could maintain their shape 15 minutes after printing.

Table 3.9. Total final height obtained for mix designs after buildability test.

Samples	**Total height (mm) at t(min) time intervals**					
	T=0	**T=5**	**T=15**	**T=30**	**T=60**	**T=120**
CONTROL (0.15%)	87.0	86.8	86.8	86.8	86.8	86.8
CONTROL_FA (0.15%)	83.5	83.3	83.3	83.3	83.3	83.3
NM_1_FA (0.15%)	92.8	92.8	92.8	92.8	92.8	92.8
SEP_0.5_FA (0.15%)	86.5	86.0	86.0	86.0	86.0	86.5

Table 3.10. Percent change of height occurred for different samples at the buildability test.

Samples	Height loss (%) at t(min) time intervals					
	T=0	**T=5**	**T=15**	**T=30**	**T=60**	**T=120**
CONTROL (0.15%)	100	0.29	0.57	0.57	0.57	0.57
CONTROL_FA (0.15%)	100	0.89	1.19	1.19	1.19	1.19
NM_1_FA (0.15%)	100	0.27	0.27	0.27	0.27	0.27
SEP_0.5_FA (0.15%)	100	0.29	0.86	0.86	0.86	0.86

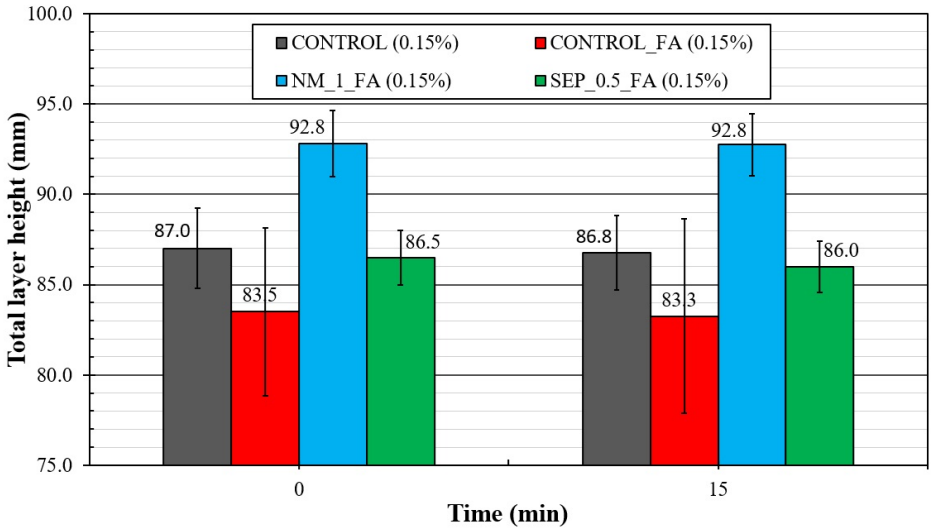

Figure 3.16. Total height of the samples at the beginning and end of the buildability test.

3.3. Hardened State Test Results

3.3.1. Compressive Strength Test Results

A controlled compressive strength test was performed on 4-layer printed specimens, prepared at 5 and 30 min time intervals at 7 and 28 days. The results were

compared with the compressive strength test results of cast specimens which were previously obtained for the same mixes [65]. The average compressive strength test results for 5 and 30 min time intervals with associated standard deviation derived from three samples are shown in Figure 3.17 and Figure 3.18, respectively. It is clear from these figures that the compressive strength of 28-day samples printed with 5 min time intervals decreased by about 26% and 11%, and similarly, the compressive strength of 28-day samples printed with 30 min time intervals decreased by about 25% and 20% when 1% of NM and SEP are added, respectively.

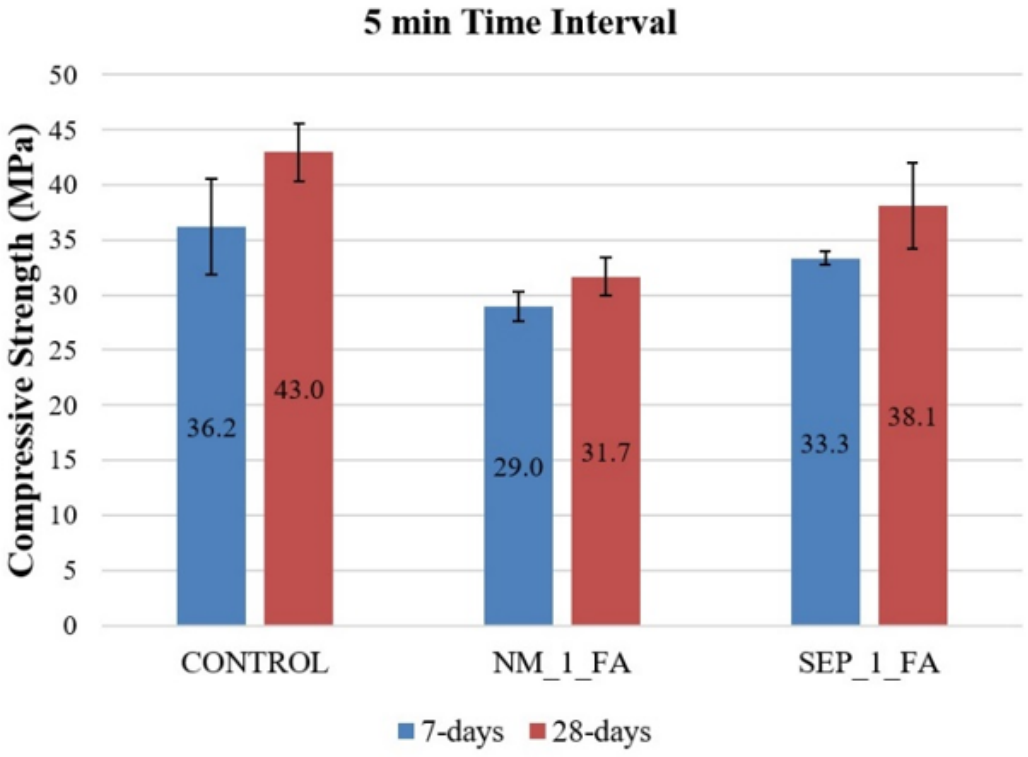

Figure 3.17. Compressive strength of printed samples with 5 min time intervals at 28 days.

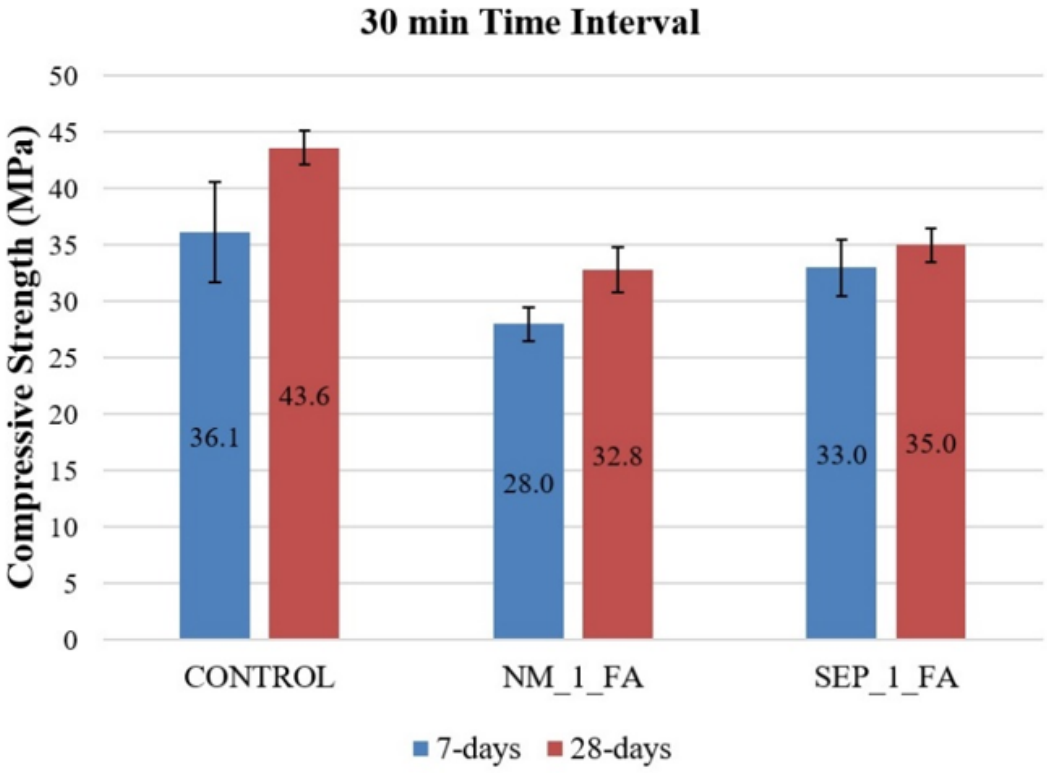

Figure 3.18. Compressive strength of printed samples with 30 min time intervals at 28 days.

By a simple comparison between the compressive strength of printed samples at 5 and 30 min time intervals in Figure 3.19, it can be seen that increasing the time gap in extruding layers from 5 to 30 min did not have any meaningful effect on the compressive strength of the samples.

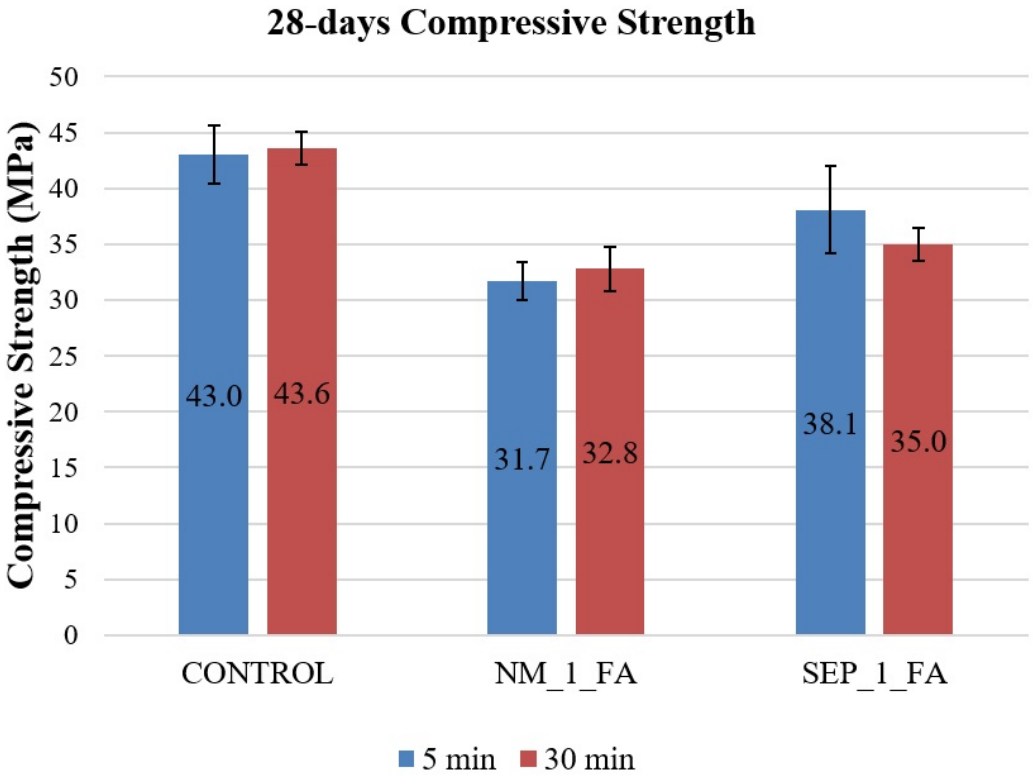

Figure 3.19. Compressive strength comparison between 5/30 min time interval.

Then compressive strength of cast and printed specimens was compared in Figure 3.20. As it was expected, the compressive strength of the printed specimens was considerably lower than the cast ones. The compressive strength of printed samples containing 1% of NM and SEP was reduced by 34% and 28% compared to their corresponding cast samples, respectively.

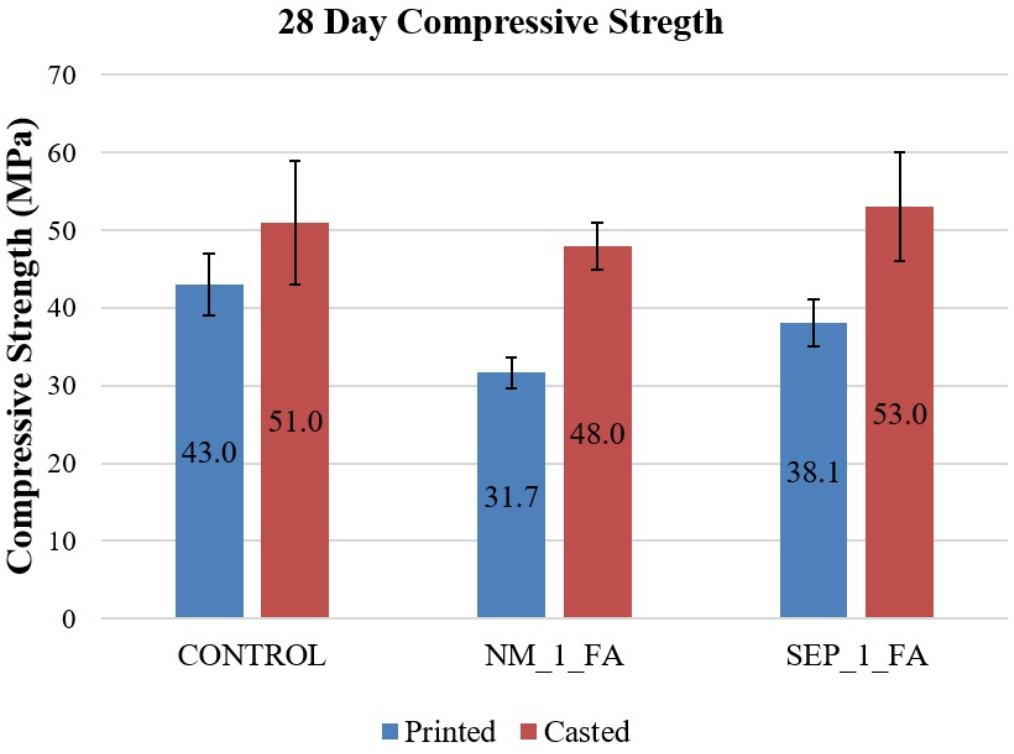

Figure 3.20. Compressive strength comparison between cast/printed samples.

As a final step of the compressive strength test, the specimens' failure pattern was analyzed carefully by ImageJ Software to highlight the cracks in order to recognize crack development and failure patterns in all samples [66]. Photos were taken from both the x-z and y-z planes according to the schematic side view shown in Figure 3.21. It should be noted that the load was applied in the z-direction.

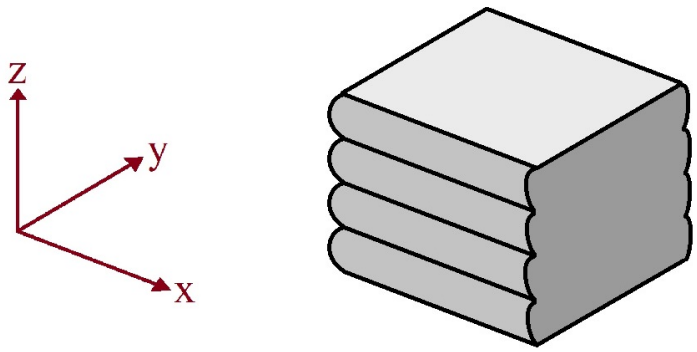

Figure 3.21. Schematic view of prepared samples.

Based on the results obtained from processed images shown in Figure 3.22, almost all of the compression failure cracks developed and propagated in a vertical direction over the height of the samples. Moreover, in the y-z plane of the samples, the majority of failure cracks propagated close to the side of the samples, while in the x-z plane, cracks developed almost all around the section in a random manner without a concentration in a specific zone. Finally, it can be seen from the failure pattern in the y-z plane that cracks propagated continuously, but failure cracks developed in a discrete manner in the x-z plane of the majority of the samples while passing through the interlayer zone. This might be due to the existence of the interlayer and cold joint resulting from an imposed 30 min time interval during the printing of the layers.

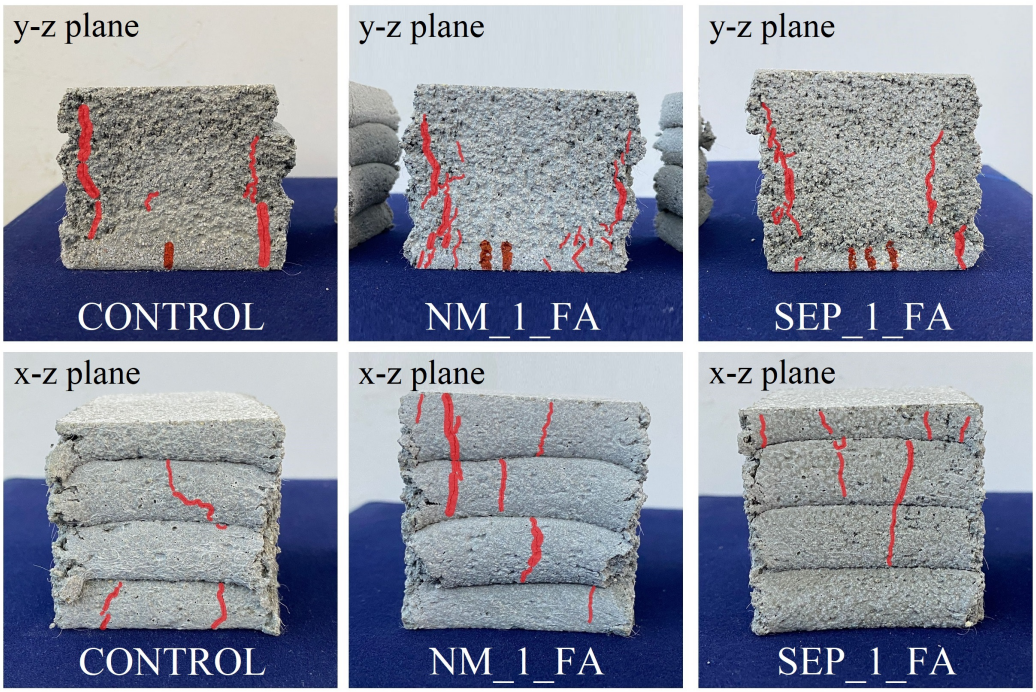

Figure 3.22. Section view of the crushed specimens under compression test and crack development pattern in y-z and x-z planes.

3.3.2. Interlayer Bonding Test Results

3.3.2.1. Interlayer bond strength dog bone shaped specimens. In the beginning, dog-bone-shaped specimens were evaluated by dividing the maximum tensile strength by

the cross-section area of the specimen. Based on the obtained results shown in Figure 3.23, it implies that the use of PA fiber and FA improved the interlayer bonding considerably, and the addition of 1% NM improved the interlayer bonding slightly.

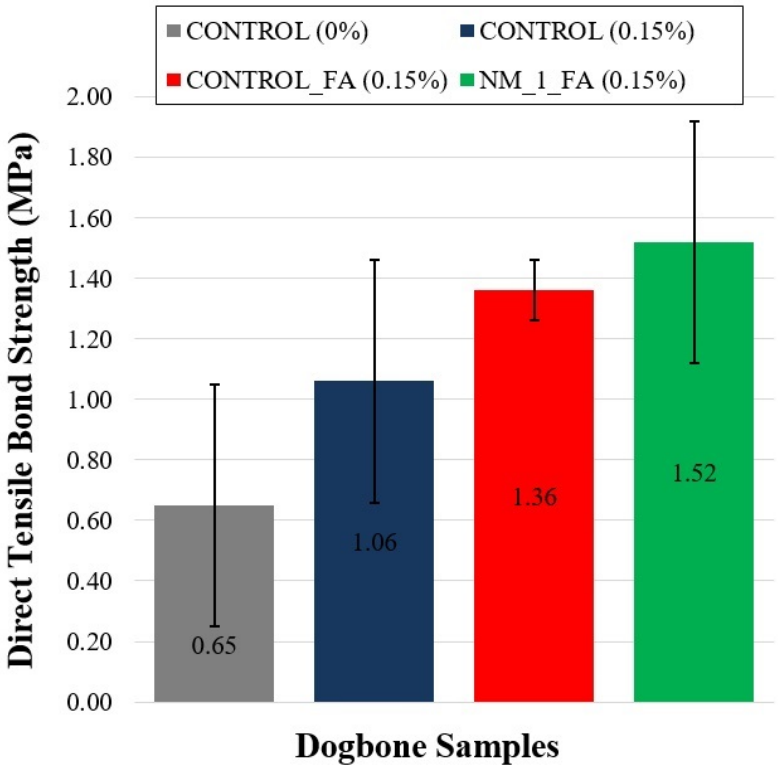

Figure 3.23. Interlayer bonding test results for dog-bone-shaped samples.

3.3.2.2. Interlayer bond strength of the printed specimens. Then samples were printed in order to investigate the bond strength of printed specimens and cement paste was applied on interlayer to improve bonding. Results of the experiments before improvement (application of cement paste layer) for series A samples are shown in Figure 3.24. Similar to the casting method, the addition of 0.15% fiber improved interlayer bonding strength by 22%. This implies the contribution of PA fibers to interlayer bonding. No significant contribution from FA addition was observed. The addition of clay enhanced the bonding in the interlayer section. The addition of 0.5% SEP and 1% NM improved the interlayer bonding by 13% and 23%, respectively. It was not possible to print SEP_1_FA by using the caulking gun, therefore results for the interlayer bond strength

of this mix could not be obtained. To conclude, it can be said that with the use of nano clays, the voids were filled and a denser mortar was obtained. As a result, interlayer bond strength was increased, since the effective surface area in the interlayer section was improved. In addition, the surface moisture of the printed layers decreased rapidly due to the high evaporation rate, which reduced the interlayer bond strength of the filaments considerably. But NM as nano-clay is reported that can reduce the loss of surface moisture [67]. As a result, water evaporation from the surface of the printed filament decreased and the interlayer bonding strength of the NM-containing samples improved.

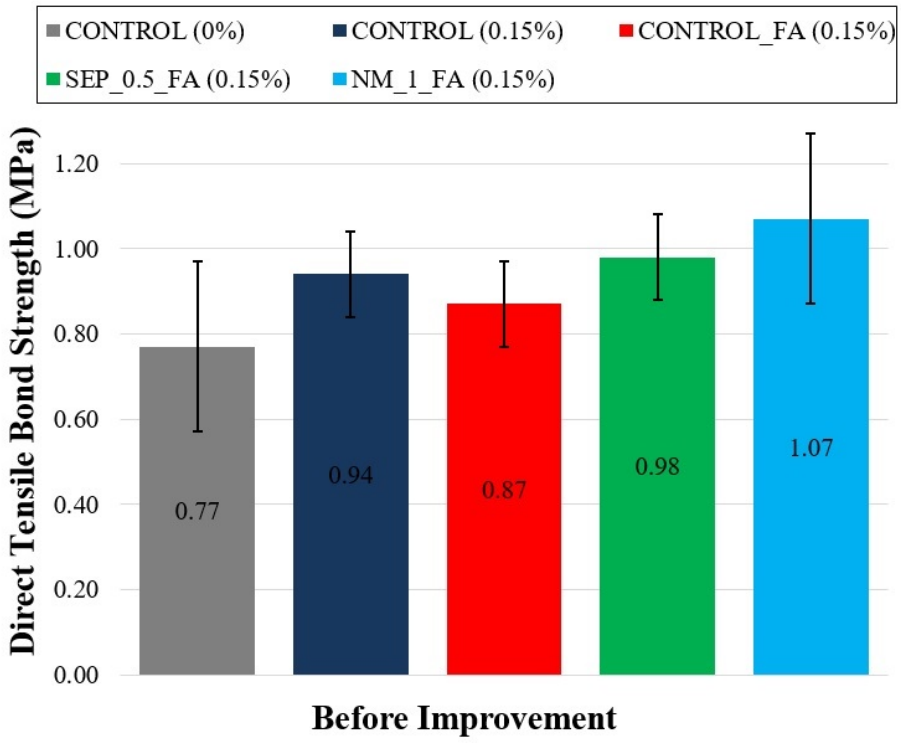

Figure 3.24. Interlayer bonding result for the printed samples-the time gap between the 2 layers was 30 min.

Cement paste was applied on the interlayer of series B samples as it was explained before to improve the binding between the layers. Based on the results illustrated in Figure 3.25, the bonding strength in all samples was improved as it was expected. Compared to the results obtained in Figure 3.24, the interlayer bonding strength of

the CONTROL sample was enhanced by 50% as the highest increase. In the same manner, fiber-containing samples including CONTROL, CONTROL_FA, SEP_0.5_FA, and NM_1_FA also got benefitted from paste application and showed an increase in their interlayer bonding strength by 39%, 39%, 32%, and 24%, respectively, shown in Figure 3.26. It can be observed that the fiber-containing samples' interlayer bonding strength was almost the same (approx- 1.3 MPa) after improving the interlayer by cement paste application.

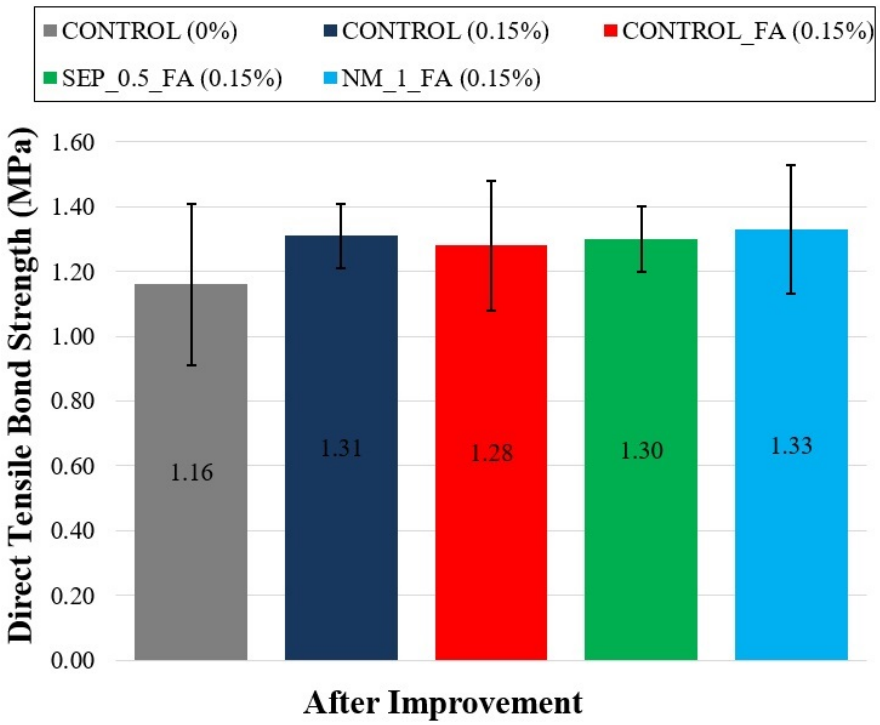

Figure 3.25. Interlayer bonding results for the printed samples after improvement of interlayer by application of cement paste (15 minutes after the printing of the 1st layer) time gap between the 2 layers was 30 min.

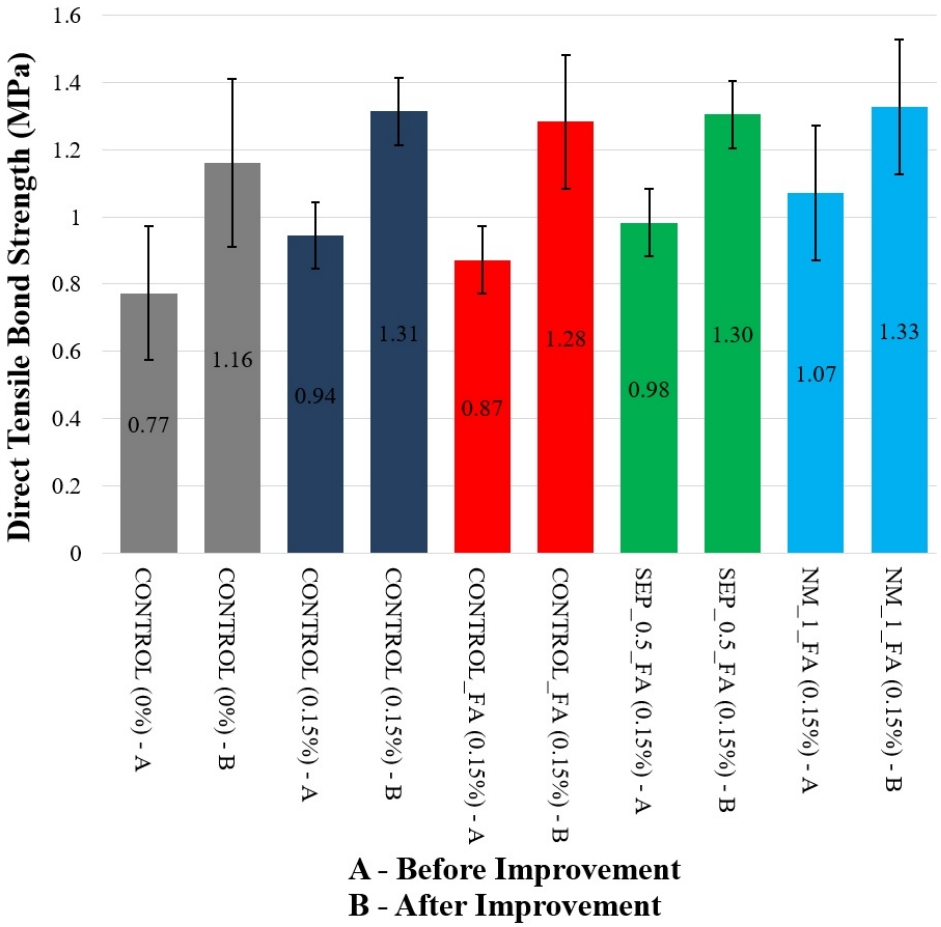

Figure 3.26. Interlayer bonding results for the printed samples before and after improvement of interlayer by application of cement paste (15 minutes after the printing of the 1st layer) time gap between the 2 layers was 30 min.

In order to understand the influence of time interval on interlayer bonding strength, the time gap decreased to 0 min. It means that the second layer was printed immediately on the first layer to generate samples without any time gap between the layers. CONTROL sample was investigated in this experiment, and obtained results were shown in Figure 3.27. As it was expected, the interlayer bonding strength of the CONTROL sample without the printing time gap was improved by 130% and reached 2.16 MPa which was more than twice the bond strength of the sample with 30 min time interval.

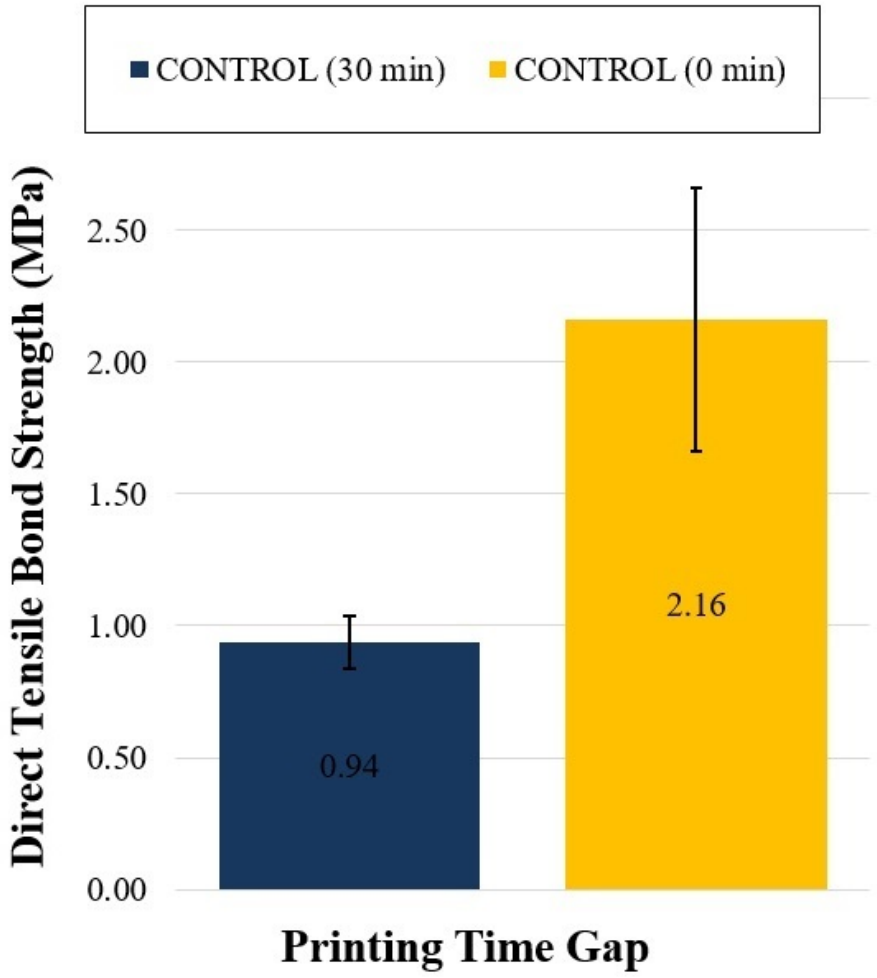

Figure 3.27. The effect of printing time gap on interlayer bonding strength-control specimen.

Figure 3.28(a) shows the specimen under uniaxial tensile loading, Figure 3.28(b) displays the printed sample after tensile failure. It is obvious from Figure 3.28(c) that the sample separated from the interlayer section. By analyzing the failure sections, it was observed that, almost all of the improved specimens separated from the interlayer. This means that spite the improvement of the interlayer bond strength of the series B specimens by application of the cement paste, still interlayer bond strength is weaker than the tensile strength of the printed cement-based mortar.

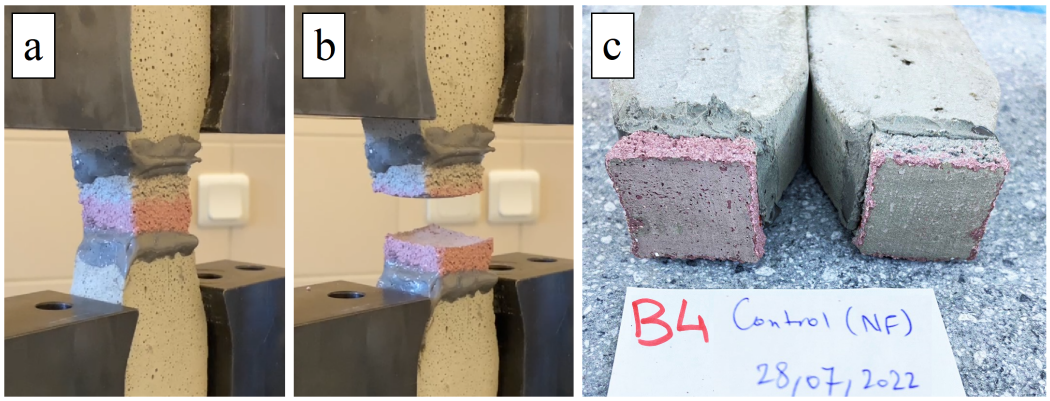

Figure 3.28. Uniaxial tensile test result, (a) under uniaxial tensile loading, (b) tensile failure, (c) interlayer section after tensile failure.

To conclude the results of these experiments imply that the time gap in 3DCP plays a significant role in bonding characteristics, which as it increases, interlayer bonding strength decreases considerably. But by application of cement paste between the layers about 24% to 39% of bonding strength can be compensated.

3.3.3. Flexural Strength Test Results

3.3.3.1. Flexural strength of the cast specimens. In the beginning, cast specimens wit-h different dosages of PA fibers were evaluated. CONTROL mix was cast with 0.10%, 0.15%, 0.20%, and 0.25% of PA fiber by weight of the binder, accordingly and 3-point bending tests were performed on 7-day specimens. Based on the obtained results shown in Figure 3.29, increasing fiber content from 0.10% to 0.25%, did not have a significant impact on the flexural properties of the sample. However, a slight decrease in flexural strength was recognized with a higher amount of fiber content. This might be due to considerable flowability reduction in high fiber contents, which may increase entrapped air void volume inside the fresh mortar, and as a result, mechanical properties are negatively affected due to more porosity [68]. Therefore, the PA fiber content increase did not have a notable effect on the flexural strength of the cast specimens.

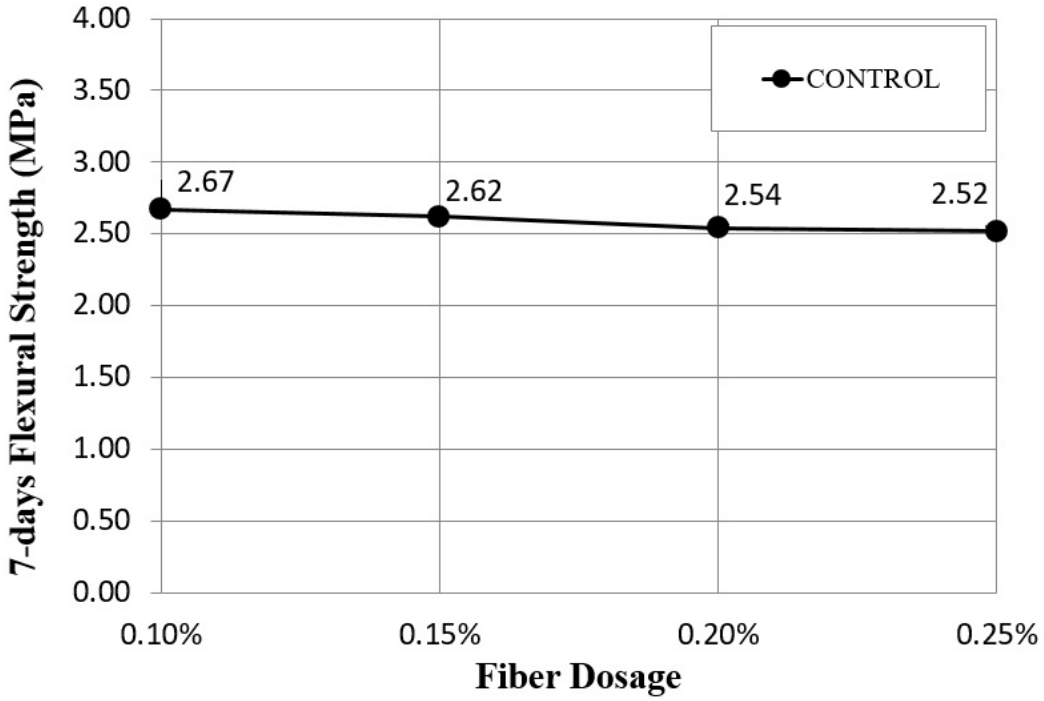

Figure 3.29. Fiber content effect on the flexural strength of cast sample.

3.3.3.2. Flexural Strength of the Printed Specimens. Printed beams with 0.15% fiber content were tested under a three-point bending test. Figure 3.30 depicts the images taken from all 2-layer beams 28 days after printing prior to conducting the flexural test. Fracture failure of the beam specimens after the three-point bending test is shown in Figure 3.31. Based on the obtained results shown in Figure 3.32, FA addition caused a slight decrease in the flexural strength of the CONTROL_FA sample at 28-day age. Based on the results shown in Table 3.11, replacing cement with 20% FA does not have any contribution to the flexural properties of 3D-printed mortar for the first 28 days [69, 70]. On the other hand, the addition of 1% NM and 0.5 SEP improved the flexural properties of printed beams by 9.6% and 19.6%, respectively. Nanoclays improve the hydration process of cement and support pozzolanic reaction by consuming calcium hydroxide and provide better microstructure by filling micro pores of the matrix which all leads to improving flexural strength of SEP and NM-containing samples [71, 72].

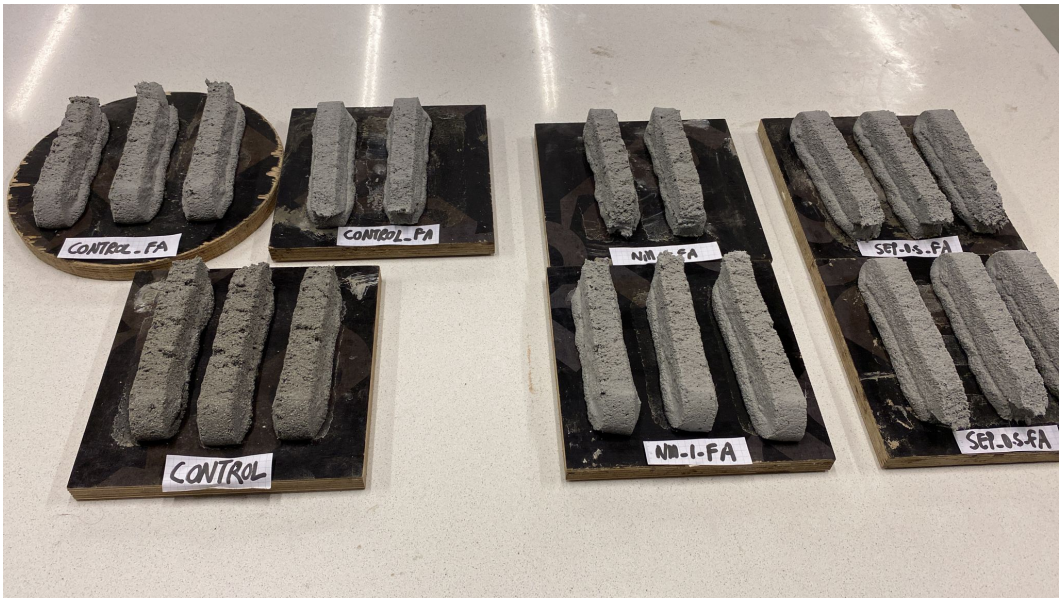

Figure 3.30. Printed beams ready for the 3-point bending test.

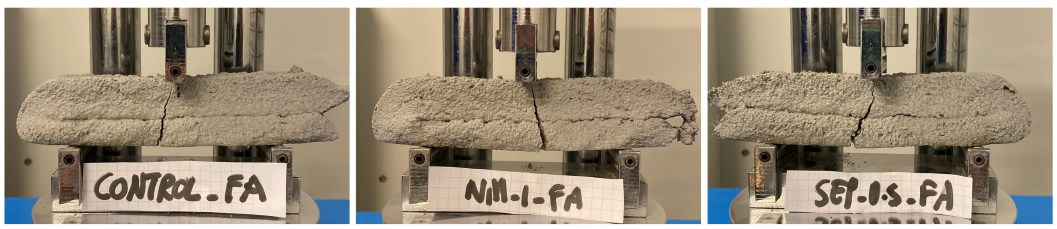

Figure 3.31. Fracture failure of the printed beams after conducting three-point bending test.

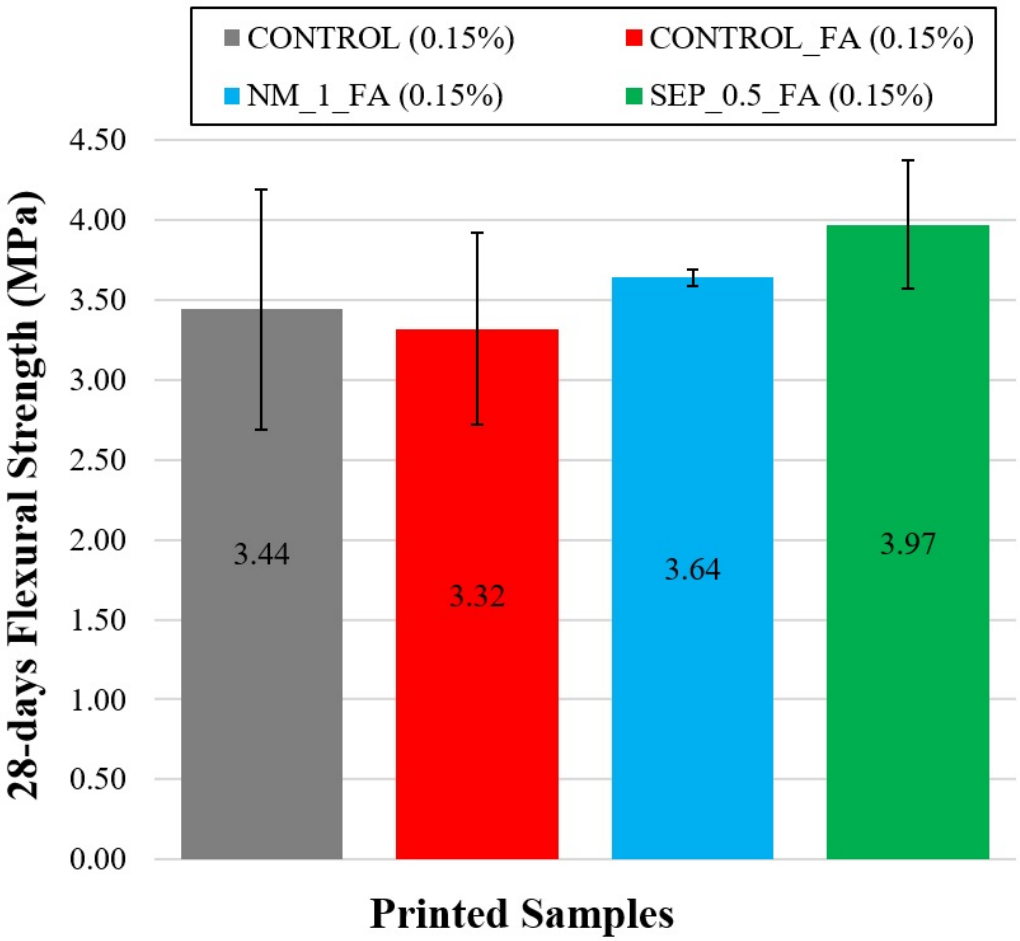

Figure 3.32. Flexural strength of the printed samples.

Table 3.11. Flexural strength test results of samples at 28-day age.

Samples	**Fly ash (%)**	**Flexural strength at 28 d (MPa)**
CONTROL (0.15%)	0	3.44
CONTROL_FA (0.15%)	20%	3.32
NM_1_FA (0.15%)	20%	3.64
SEP_0.5_FA (0.15%)	20%	3.97

4. CONCLUSION

This study was conducted to investigate the effect of nano clays and PA fiber on the rheological and mechanical properties of cementitious mortar tailored for 3DP. Two different types of clay were used in this study to evaluate their influence on the behavior of the concrete in the fresh and hardened state of designed mortars. Moreover, the partial replacement of cement by FA was investigated to explore the sustainability in 3DCP and study the effect of FA on different characteristics of printed concrete. Some experiments were done with both casting and printing techniques in order to do a comparative study and evaluate printing influence on properties of the designed mortar. Based on the obtained results:

- PA fibers are evenly distributed inside the cement-based mortar whether by conducting a dry mechanical mix inside the cement or introducing it gradually to the water during performing a continuous mix utilizing a magnetic stirrer. Distributing fiber in water is more suitable for lower contents of PA fiber, but at higher rates larger than 0.125% (by weight of binder amount), PA fiber clumps during mechanical mixing with water. On the other hand, the dry mix method showed excellent distribution for higher contents of PA fibers.
- Through investigation and based on the observation, uniform distribution of PA fibers inside cement-based mortar is not a serious challenge in lower dosages, however suitable dispersion methods should be implemented for higher than 0.15% dosages.
- Introducing 12 mm length PA fibers at a rate of 0.150% inside the designed cement-based mortar did not cause any change in the mortar's extrudability properties, so all designed mixtures were extruded without clogging inside the nozzle during printing by the robot as well as printing manually by caulking gun.
- Substituting 20% of cement by FA increased the flow as it was expected, but it accelerated the flow loss considerably in the initial 60 minutes after completing the mixing.

- The addition of 1% NM/SEP caused a decrease in flowability. However, NM addition controls the flow loss and maintains the flow better than SEP containing sample over a 2-hour period. Moreover, SEP content increase from 0.5% to 1% accelerated the flow loss considerably compared to NM increase in the same range.
- Although increasing PA fiber content decreased workability and hindered the flow due to its hydrophilic nature and special geometry, the flow loss was decelerated in higher contents of fiber.
- The flowability of NM containing sample showed high sensitivity to fiber content increase from 0.05% to 0.125% and lost its workability considerably in all time intervals compared to SEP containing mixture which did not show a significant change in its workability against fiber content growth in the same range.
- Based on the results of the buildability test, NM and SEP addition improves cohesion and appearance, and results in uniform shape of the structure. Moreover, it was observed that buildability characteristics were decreased after a 20% substitution of cement by FA. The height change trend stopped 15 min after printing which means the designed cement-based mortar obtained its final shape 15 min after printing.
- The 28-day compressive strength of printed samples decreased with the addition of NM and SEP. Increasing the time gap between printing the layers did not impact the compressive strength of the mixtures. As it was expected, printed specimens showed lower compressive strength compared to conventionally cast ones.
- Evaluating the failure patterns of the compression test demonstrated that the failure cracks developed and propagated vertically. Moreover, in the cross-section (perpendicular to the printing direction) of printed cubic specimens, failure cracks propagated vertically close to the sides of the specimens in a continuous way, while in side section (parallel to the printing direction) of the specimens, cracks propagated in all around the section randomly in a discrete manner while passing through the interlayer zone.
- Interlayer bonding strength did not change considerably after substituting cement with 20% of FA, but fiber addition enhanced bonding in the interlayer zone. In

the same way, the addition of SEP and NM improved the interlayer bonding. Moreover, cement paste application on the layers enhanced the bonding properties of all mix designs in the interlayer zone by about 25 to 40%. Then, it is concluded that by reducing the printing time gap to 0 min, interlayer bonding can be improved by 130% compared to the specimen with a 30 min time interval, which proves time gap has a significant effect on interlayer bonding properties of the printed specimens.

- The fiber ratio increase does not have a special effect on the flexural strength of the printed samples, but the addition of NM and SEP improved flexural properties by about 10 and 20%, respectively.

To conclude, PA fiber proved to be a convenient choice for 3DCP since they were distributed easily and did not cause any problem during extrusion. However, it was observed that higher dosages of PA fiber adversely affected workability but decreased flow loss rate. On the other hand, FA demonstrated efficiency in enhancing rheological characteristics, but its potential side-effects on buildability and flow loss acceleration must be taken into consideration. Although the addition of NM and SEP as clays resulted in a slight decrease in compressive strength, their positive impact on 3DCP was evident through improved buildability, cohesion, layer appearance, interlayer bonding, and flexural strength. The hydrophilic nature of NM and especially SEP, as Nano clays, led to reduced workability, but NM exhibited a deceleration in the flow loss rate over time. On the other hand, the workability of the NM-containing sample due to containing excessive water, proved to be more sensitive to increases in fiber content. Notably, while the printing time gap between layers did not affect compressive strength, it played a crucial role in the strength of interlayer bonding. To address this, a practical solution was devised in this research, involving the application of cement paste in the interlayer zone to enhance interlayer bonding properties.

4.1. Future Work

Cement replacement by FA did not exceed 20% in this research. Due to its benefits for 3DCP, higher content of FA usage can be investigated in order to make the printed concrete industry greener.

Other materials' application in the interlayer zone may be investigated to improve interlayer bonding properties. Cement paste was applied in the middle of the time interval according to the scope of this study. It is suggested to investigate its application in different time intervals especially just before applying the subsequent layer. Moistening the interlayer may also improve the bonding since it was observed that after 30 min the surface of the printed layer loses its moisture considerably, so a lower w/c ratio cement paste might also show a similar effect to the higher ratios.

Although supplementary materials like Nano clays improve the properties of printed concrete from various perspectives, their availability and price should be taken into account. Moreover, the specific size of clay was utilized in this study, but due to their hydrophilic characteristics, the different particle sizes of NM and SEP may change the rheological behavior of the designed mortar, as a recommendation for future research.

REFERENCES

1. El-Sayegh, S., L. Romdhane and S. Manjikian, "A Critical Review of 3D Printing in Construction: Benefits, Challenges, and Risks", *Archives of Civil and Mechanical Engineering*, Vol. 20, No. 2, pp. 1-25, 2020.

2. Hossain, M. A., A. Zhumabekova, S. C. Paul and J. R. Kim, "A Review of 3D Printing in Construction and Its Impact on the Labor Market", *Sustainability (Switzerland)*, Vol. 12, No. 20, pp. 1-21, 2020.

3. Olsson, N. O. E., E. Arica, R. Woods and J. A. Madrid, "Industry 40 in a Project Context: Introducing 3D Printing in Construction Projects", *Project Leadership and Society*, Vol. 2, pp. 100033-100053, 2021.

4. Mohan, M. K., A. V. Rahul, G. De Schutter and K. Van Tittelboom, "Extrusion-Based Concrete 3D Printing from a Material Perspective: A State-of-the-Art Review", *Cement and Concrete Composites*, Vol. 115, pp. 103855-103870, 2021.

5. Pan, Y., Y. Zhang, D. Zhang and Y. Song, "3D Printing in Construction: State of the Art and Applications", *International Journal of Advanced Manufacturing Technology*, Vol. 115, No. 5-6, pp. 1329-1348, 2021.

6. Tay, Y. W. D., B. Panda, S. C. Paul, N. A. Noor Mohamed, M. J. Tan and K. F. Leong, "3D Printing Trends in Building and Construction Industry: A Review", *Virtual and Physical Prototyping*, Vol. 12, No. 3, pp. 261-276, 2017.

7. Du Plessis, A., A. J. Babafemi, S. C. Paul, B. Panda, J. P. Tran, and C. Broeckhoven, "Biomimicry for 3D Concrete Printing: A Review and Perspective", *Additive Manufacturing*, Vol. 38, pp. 101823-101833, 2021.

8. Zhang, C., V. N. Nerella, A. Krishna, S. Wang, Y. Zhang, V. Mechtcherine and N. Banthia, "Mix Design Concepts for 3D Printable Concrete: A Review", *Cement*

and Concrete Composites, Vol. 122, pp. 104155-104170, 2021.

9. Rahul, A.V., M. Santhanam, H. Meena and Z. Ghani, "3D Printable Concrete: Mixture Design and Test Methods", *Cement and Concrete Composites*, Vol. 97, pp. 13-23, 2019.

10. Hosseini, E., M. Zakertabrizi, A. H. Korayem and G. Xu, "A Novel Method to Enhance the Interlayer Bonding of 3D Printing Concrete: An Experimental and Computational Investigation", *Cement and Concrete Composites*, Vol. 99, pp. 112-119, 2019.

11. Marchment, T., J. Sanjayan and M. Xia, "Method of Enhancing Interlayer Bond Strength in Construction Scale 3D Printing with Mortar by Effective Bond Area Amplification", *Materials and Design*, Vol. 169, pp. 107684-107697, 2019.

12. Ma, G., N. M. Salman, L. Wang and F. Wang, "A Novel Additive Mortar Leveraging Internal Curing for Enhancing Interlayer Bonding of Cementitious Composite for 3D Printing", *Construction and Building Materials*, Vol. 244, pp. 118305-118325, 2020.

13. Van Der Putten, J., M. Azima, P. Van den Heede, T. Van Mullem, D. Snoeck, C. Carminati and J. Hovind, "Neutron Radiography to Study the Water Ingress via the Interlayer of 3D Printed Cementitious Materials for Continuous Layering", *Construction and Building Materials*, Vol. 258, pp. 119587-119600, 2020.

14. Zareiyan, B. and B. Khoshnevis, "Effects of Interlocking on Interlayer Adhesion and Strength of Structures in 3D Printing of Concrete", *Automation in Construction*, Vol. 83, pp. 212-221, 2017.

15. Hamidi, F. and F. Aslani, "Additive Manufacturing of Cementitious Composites: Materials, Methods, Potentials and Challenges", *Construction and Building Materials*, Vol. 218, pp. 582-609, 2019.

16. Lu, B., Y. Weng, M. Li, Y. Qian, K. F. Leong, M. J. Tan and S. Qian, "A Systematical Review of 3D Printable Cementitious Materials", *Construction and Building Materials*, Vol. 207, pp. 477-490, 2019.

17. Panda, B. and M. J. Tan, "Rheological Behavior of High Volume Fly Ash Mixtures Containing Micro Silica for Digital Construction Application", *Materials Letters*, Vol. 237, pp. 348-351, 2019.

18. Nematollahi, B., M. Xia and J. Sanjayan, "Current Progress of 3D Concrete Printing Technologies", *International Symposium on Automation and Robotics in Construction and Mining (ISARC 2017)*, Taipei, Taiwan, No. 5, pp. 260-267, 2017.

19. Khan, M. A., "Mix Suitable for Concrete 3D Printing: A Review", *Materials Today: Proceedings*, Vol. 32, pp. 831-837, 2020.

20. Arunothayan, A. R., B. Nematollahi, R. Ranade, S. H. Bong, J. G. Sanjayan and K.H. Khayat, "Fiber Orientation Effects on Ultra-High Performance Concrete Formed by 3D Printing", *Cement and Concrete Research*, Vol. 143, pp. 106384-106394, 2021.

21. Le, T. T., S. A. Austin, S. Lim, R. A. Buswell, R. Law, A. G. F. Gibb and T. Thorpe, "Hardened Properties of High-Performance Printing Concrete", *Cement and Concrete Research*, Vol. 42, No. 3, pp. 558-566, 2012.

22. Panda, B., S. Chandra Paul and M. Jen Tan, "Anisotropic Mechanical Performance of 3D Printed Fiber Reinforced Sustainable Construction Material", *Materials Letters*, Vol. 209, pp. 146-149, 2017.

23. Bos, F. P., E. Bosco and T. A. M. Salet, "Ductility of 3D Printed Concrete Reinforced with Short Straight Steel Fibers", *Virtual and Physical Prototyping*, Vol. 14, No. 2, pp. 160-174, 2019.

24. Arunothayan, A. R., B. Nematollahi, R. Ranade, S. H. Bong and J. Sanjayan, "De-

velopment of 3D-Printable Ultra-High Performance Fiber-Reinforced Concrete for Digital Construction", *Construction and Building Materials*, Vol. 257, pp. 119546-119566, 2020.

25. Güler, S., "The Effect of Polyamide Fibers on the Strength and Toughness Properties of Structural Lightweight Aggregate Concrete", *Construction and Building Materials*, Vol. 173, pp. 394-402, 2018.

26. Marchon, D., S. Kawashima, H. Bessaies-Bey, S. Mantellato and S. Ng, "Hydration and Rheology Control of Concrete for Digital Fabrication: Potential Admixtures and Cement Chemistry",*Cement and Concrete Research*, Vol. 112, pp. 96-110, 2018.

27. Kim, J. H., M. Beacraft and S. P. Shah, "Effect of Mineral Admixtures on Formwork Pressure of Self-Consolidating Concrete", *Cement and Concrete Composites*, Vol. 32, No. 9, pp. 665-671, 2010.

28. Quanji, Z., G. R. Lomboy and K. Wang, "Influence of Nano-Sized Highly Purified Magnesium Alumino Silicate Clay on Thixotropic Behavior of Fresh Cement Pastes", *Construction and Building Materials*, Vol. 69, pp. 295-300, 2014.

29. Kawashima, S., M. Chaouche, D. J. Corr and S. P. Shah, "Rate of Thixotropic Rebuilding of Cement Pastes Modified with Highly Purified Attapulgite Clays", *Cement and Concrete Research*, Vol. 53, pp. 112-118, 2013.

30. Aydın, E. M., B. Kara, Z. B. Bundur, N. Özyurt, O. Bebek and M. A. Gülgün, "A Comparative Evaluation of Sepiolite and Nano-Montmorillonite on the Rheology of Cementitious Materials for 3D Printing", *Construction and Building Materials*, Vol. 350, pp. 128935-128950, 2022.

31. Rahul, A. V. and M. Santhanam, "Evaluating the Printability of Concretes Containing Lightweight Coarse Aggregates", *Cement and Concrete Composites*, Vol.

109, pp. 103570-103585, 2020.

32. Ma, G., Y. Li, L. Wang, J. Zhang and Z. Li, "Real-Time Quantification of Fresh and Hardened Mechanical Property for 3D Printing Material by Intellectualization with Piezoelectric Transducers", *Construction and Building Materials*, Vol. 241, pp. 117982-117997, 2020.

33. Zhang, X., M. Li, J. H. Lim, Y. Weng, Y. W. D. Tay, H. Pham and Q. C. Pham, "Large-Scale 3D Printing by a Team of Mobile Robots", *Automation in Construction*, Vol. 95, pp. 98-106, 2018.

34. Alchaar, A. S. and A. K. Al-Tamimi, "Mechanical Properties of 3D Printed Concrete in Hot Temperatures", *Construction and Building Materials*, Vol. 266, pp. 120991-120999, 2021.

35. Soltan, D. G. and V. C. Li, "A Self-Reinforced Cementitious Composite for Building-Scale 3D Printing", *Cement and Concrete Composites*, Vol. 90, pp. 1-13, 2018.

36. Ogura, H., V. N. Nerella and V. Mechtcherine, "Developing and Testing of Strain-Hardening Cement-Based Composites (SHCC) in the Context of 3D-Printing", *Materials*, Vol. 11, No. 8, pp. 1-18, 2018.

37. Shakor, P., S. Nejadi and G. Paul, "A Study into the Effect of Different Nozzles Shapes and Fibre-Reinforcement in 3D Printed Mortar", *Multidisciplinary Digital Publishing Institute*, Vol. 12, No. 10, pp. 1708-1738, 2019.

38. British Standards Institution (BSI), "Methods of TestingComposition, Specifications and Conformity Criteria for Common Cements", *British Standards Institution (BSI) Standards Publication*, Vol. 1, pp. 50-70, 2011.

39. Weng, Y., B. Lu, M. J. Tan and S. Qian, "Rheology and Printability of Engineered Cementitious Composites - A Literature Review", *Proceedings of the International*

Conference on Progress in Additive Manufacturing, Butit Batok, Singapor, Vol. 1, No. F1290, pp. 427-432, 2016.

40. Bhattacherjee, S., A. S. Basavaraj, A. V. Rahul, M. Santhanam, R. Gettu, B. Panda, E. Schlangen, "Sustainable Materials for 3D Concrete Printing", *Cement and Concrete Composites*, Vol. 122, pp. 104156-104170, 2021.

41. Kazemian, A., X. Yuan, E. Cochran and B. Khoshnevis, "Cementitious Materials for Construction-Scale 3D Printing: Laboratory Testing of Fresh Printing Mixture", *Construction and Building Materials*, Vol. 145, pp. 639-647, 2017.

42. Hosseini, P., A. Afshar, B. Vafaei, A. Booshehrian, E. Molaei Raisi and A. Esrafili, "Effects of Nano-Clay Particles on the Short-Term Properties of Self-Compacting Concrete", *European Journal of Environmental and Civil Engineering*, Vol. 21, No. 2, pp. 127-147, 2017.

43. Liu, P., M. Du, P. Clode, H. Li, J. Liu and Y. K. Leong, "Surface Chemisty, Microstructure and Rheology of Thixotropic 1-D Sepiolite Gels", *Clays and Clay Minerals*, Vol. 68, No. 1, pp. 9-22, 2020.

44. Sheet, P. D., "Sika℞ViscoCrete℞-3110", *Inorganic Materials*, No. January, pp. 1-3, 2017.

45. Wheeler, L., "Standard Practice for Supplementation", *Journal of Human Lactation*, Vol. 14, No. 2, pp. 147-160, 1998.

46. Kim, H., G. Kim, N. Gucunski, J. Nam and J. Jeon, "Assessment of Flexural Toughness and Impact Resistance of Bundle-Type Polyamide Fiber-Reinforced Concrete", *Composites Part B: Engineering*, Vol. 78, pp. 431-446, 2015.

47. Josef Fládra, P. B. and I. B., "Evaluation of Steel Fiber Distribution in Concrete by Computer Aided Image Analysis", *Composite Materials and Engineering*, Vol. 1, pp. 49-70, 2019.

48. Le, T. T., S. A. Austin, S. Lim, R. A. Buswell, A. G. F. Gibb and T. Thorpe, "Mix Design and Fresh Properties for High-Performance Printing Concrete", *Materials and Structures/Materiaux et Constructions*, Vol. 45, No. 8, pp. 1221-1232, 2012.

49. American Society for Testing and Materials (ASTM) C230, "Standard Specification for Flow Table for Use in Tests of Hydraulic Cement 1", *Annual Book of American Society for Testing and Materials (ASTM) Standards*, pp. 4-9, 2010.

50. Fuyan, L., Z. Dongliang , H. Xiaohui, S. L. and Q. Zhang, "Applied Sciences Overview of the Development of 3D-Printing Concrete", *Applied Sciences*, Vol. 11, No. 21, pp. 9822-9840, 2021.

51. Chang, Z., Y. Xu, Y. Chen, Y. Gan, E. Schlangen and B. Šavija, "A Discrete Lattice Model for Assessment of Buildability Performance of 3D-Printed Concrete", *Computer-Aided Civil and Infrastructure Engineering*, Vol. 36, No. 5, pp. 638-655, 2021.

52. Cui, H., Y. Li, X. Cao, M. Huang, W. Tang and Z. Li, "Experimental Study of 3D Concrete Printing Configurations Based on the Buildability Evaluation", *Applied Sciences (Switzerland)*, Vol. 12, No. 6, pp. 2939-2950, 2022.

53. American Society for Testing and Materials (ASTM) C 109/C 109M-21, "Standard Test Method for Compressive Strength of Hydraulic Cement Mortars", *Annual Book of American Society for Testing and Materials (ASTM) Standards*, Vol. 04, pp. 9-15, 2021.

54. Hassan, A. M. T., S. W. Jones and G. H. Mahmud, "Experimental Test Methods to Determine the Uniaxial Tensile and Compressive Behaviour of Ultra High Performance Fibre Reinforced Concrete(UHPFRC)", *Construction and Building Materials*, Vol. 37, pp. 874-882, 2012.

55. He, L., W. T. Chow and H. Li, "Effects of Interlayer Notch and Shear Stress on

Interlayer Strength of 3D Printed Cement Paste", *Additive Manufacturing*, Vol. 36, pp. 101390-101403, 2020.

56. Marchment, T., J. G. Sanjayan, B. Nematollahi and M. Xia, "Interlayer Strength of 3D Printed Concrete", *Materials & Design*, Vol. 169, pp. 107684-107699, 2019.

57. Babafemi, A. J., J. T. Kolawole, M. J. Miah, S. C. Paul and B. Panda, "A Concise Review on Interlayer Bond Strength in 3d Concrete Printing", *Sustainability (Switzerland)*, Vol. 13, No. 13, pp. 7137-7147, 2021.

58. Zhong, H. and M. Zhang, "3D Printing Geopolymers: A Review", *Cement and Concrete Composites*, Vol. 128, pp. 104455-104485, 2022.

59. De Santis, S., H. A. Hadad, F. De Caso y Basalo, G. de Felice and A. Nanni, "Acceptance Criteria for Tensile Characterization of Fabric-Reinforced Cementitious Matrix Systems for Concrete and Masonry Repair", *Journal of Composites for Construction*, Vol. 22, No. 6, pp. 1-14, 2018.

60. Panda, B., N. A. N. Mohamed, S. C. Paul, G. V. P. B. Singh, M. J. Tan and B. Šavija, "The Effect of Material Fresh Properties and Process Parameters on Buildability and Interlayer Adhesion of 3D Printed Concrete", *Materials*, Vol. 12, No. 13, pp. 2149-2160, 2019.

61. American Society for Testing and Materials (ASTM) C880, "Standard Test Method for Flexural Strength of Dimension Stone", *Annual Book of American Society for Testing and Materials (ASTM) Standards*, Vol. 03, pp. 98-100, 1999.

62. Rouquerol, F., J. Rouquerol and K. Sing, "Adsorption by Clays, Pillared Layer Structures and Zeolites", *Adsorption by Powders and Porous Solids*, pp. 355-399, 1999.

63. Kuranlı, Ö. F., M. Uysal and O. Canpolat, "Mechanical and Durability Properties of Slag/Fly Ash Based Alkali-Activated Concrete Reinforced with Steel,

Polypropylene and Polyamide Fibers", *European Journal of Environmental and Civil Engineering*, Vol. 26, No. 16, pp. 8390-8413, 2022.

64. Mármol, G., H. Savastano, E. de la Fuente, R. Miranda, Á. Blanco and C. Negro, "Effect of Sepiolite Addition on Fibre-Cement Based on MgO-SiO_2 Systems", *Cement and Concrete Research*, Vol. 124, pp. 105816-105846, 2019.

65. Aydın, E. M., *Extrusion and Rheology Characterization of Cement-Based Materials Containing Different Types of Clays*, M.Sc. Thesis, Özyeğin University, 2021.

66. Ye, J., C. Cui, J. Yu, K. Yu and F. Dong, "Effect of Polyethylene Fiber Content on Workability and Mechanical-Anisotropic Properties of 3D Printed Ultra-High Ductile Concrete", *Construction and Building Materials*, Vol. 281, pp. 122586-122599, 2021.

67. Pan, T., Y. Jiang, H. He, Y. Wang and K. Yin, "Effect of Structural Build-up on Interlayer Bond Strength of 3d Printed Cement Mortars", *Materials*, Vol. 14, No. 2, pp. 1-17, 2021.

68. Ramezanianpour, A. A., M. Esmaeili, S. A. Ghahari and M. H. Najafi, "Laboratory Study on the Effect of Polypropylene Fiber on Durability and Physical and Mechanical Characteristic of Concrete for Application in Sleepers", *Construction and Building Materials*, Vol. 44, pp. 411-418, 2013.

69. Wong, Y. L., L. Lam, C. S. Poon and F. P. Zhou, "Properties of Fly Ash-Modified Cement Mortar-Aggregate Interfaces", *Cement and Concrete Research*, Vol. 29, No. 12, pp. 1905-1913, 1999.

70. Upadhyay, R., V. Srivastava, A. Herbert and P. K. Mehta, "Effect of Fly Ash on Flexural Strength of Portland Pozzolona Cement Concrete", *Journal of Academia and Industrial Research*, Vol. 3, No. 5, pp. 218-220, 2014.

71. Wei, J. and C. Meyer, "Sisal Fiber-Reinforced Cement Composite with Portland

Cement Substitution by a Combination of Metakaolin and Nanoclay", *Journal of Materials Science*, Vol. 49, No. 21, pp. 7604-7619, 2014.

72. Hakamy, A., F. U. A. Shaikh and I. M. Low, "Characteristics of Nanoclay and Calcined Nanoclay-Cement Nanocomposites", *Composites Part B: Engineering*, Vol. 78, pp. 174-184, 2015.